1	Scour variability across offshore wind farms (OWFs):
2	Understanding sIdentifying site-specific scour drivers as a step
3	towards assessing potential impacts on the marine environment
4	81 1
5	Karen Garcia ^{1*} , Christian Jordan ¹ , Gregor Melling ³ , Alexander Schendel ^{1,2} , Mario Welzel ¹ , Torsten
6	Schlurmann ^{1,2}
7	¹ Leibniz University Hannover, Ludwig-Franzius-Institute for Hydraulic, Estuarine and Coastal Engineering,
8	Nienburger Str. 4, 30167 Hannover, Germany. Email: schendel@lufi.uni-hannover.de ,

39 1 Introduction & Motivation

- The expansion of renewable energy is crucial for a sustainable and independent energy supply. In order to meet the European Union's targets for expanding offshore wind energy (EU, 2020), it is necessary to develop areas with previously unveiled metoceanic and geophysical conditions. To this end, existing knowledge gaps about the interaction of individual offshore wind energy structures (OWES) or entire offshore wind farms (OWFs) with the marine environment must be closed. In general, the disturbance of the flow by an offshore structure causes scour, which might not only affect the structure's stability (Saathoff et al., 2024), but the mobilized sediment may also contribute to the overall regional sediment transport (Vanhellemont et al., 2014; Baeye and Fettweis, 2015; Rivier et al., 2016) with potential impacts on the marine environment.
- The scour process itself, is a multivariate process, which is dependent on a combination of complex hydrodynamic 48 49 and geotechnical drivers. Early studies focused on the understanding of the scour process around a pile under 50 simplified isolated hydraulic conditions, such as steady flow (e.g., Sheppard et al., 2004; Zhao et al., 2012; Sarkar 51 et al., 2014; Baykal et al., 2015), unsteady and bidirectional tidal currents (e.g. Escarameia and May1999; McGovern et al., 2014; Yao et al., 2016; Schendel et al., 2018) and waves (e.g. Sumer et al., 1992b; Carreiras et 52 53 al., 2001; Stahlmann et al., 2013). With the availability of more sophisticated experimental facilities and numerical models, research is increasingly shifting toward more complex hydrodynamic loads consisting of a combination 54 55 of waves and currents, as in the studies of Sumer and Fredsøe (2001), Qi and Gao (2014), Schendel et al. (2020), 56 Lyu et al. (2021), and Du et al. (2022) but and also towards studies addressing complex offshore structures (Welzel, 2021; Welzel et al., 2024; Sarmiento et al., 2024; Chen et al., 2025).
- Despite those advances in scour research, uncertainties remain in current scour prediction methods (Chen et al., 2024). Matutano et al. (2013) demonstrated the challenges of applying empirical formulas for maximum scour depthsdepth by comparing different methods with data from ten European OWFs, revealing overpredictions in all but two cases. The comparison highlights the fundamental challenge of accounting for complex marine flow conditions, characterized by the superposition-combined effect of multiple influencing factors, such as flow velocity, sediment coarseness, and wave-current interactions, in the prediction of scour processes using existing models (Gazi et al., 2020; Harris et al., 2023).
- 65 Compared to laboratory experiments focusing on scour processes, rather few studies are based on in-situ data, that represent the actual scour development under complex flow conditions. These studies assessed the scour at individual structures, such as monopiles (Walker, 1995; Noormets et al., 2003; Harris et al., 2004; Rudolph et al., 2004; Louwersheimer et al., 2009), and jackets (Bolle et al., 2012; Baelus et al., 2018; Harris and Whitehouse et 68 69 al., 2021), or dealt with larger datasets from entire offshore wind projects (DECC 2008; COWRIE 2010; Whitehouse et al., 2010; Whitehouse et al., 2011; Melling (2015)), covering both spatial and temporal evolution 70 71 of scour under different hydrodynamic regimes and seabed types across the North Sea and British continental shelf. In general, the amount and variety of field data collected has increased with the gradual installation of offshore wind turbines OWES. Focusing-specifically on the correlation between scour and on-site conditions, Melling (2015) analyzed the relationships between the variations of scour hole dimension within OWFs and both sedimentological and hydrodynamic parameters of 281 turbines OWES in the Outer Thames estuary. Melling's 75 (2015) study, although only covering three OWFs, represents one of the most comprehensive investigations of field related scour to date, with the highest number of structures examined so far. By comparing field data with

physical modeling experiments and literature, the study provided valuable insights into the range of observed scour
 and its controlling structural hydrodynamic, and sedimentological parameters.

In addition to local scour at individual structures, the cumulative effect of multiple structures in an OWFs can alter 80 ocean dynamics (Christiansen et al., 2022), mixing (Schultze et al., 2020), and sediment mobility, resulting in 81 changes to suspended sediment concentrations and wave-induced turbidity plumes (Vanhellemont & Ruddick, 82 83 2014). This can also lead to dynamic interactions with migrating seabed features, such as sand waves (Matthieu & Raaijmakers, 2012). Increased velocities and turbulence induced by OWFs has also the potential to affect the 84 85 marine environment, potentially leading to global erosion around the structures as well as habitat loss or gain for 86 benthic flora and fauna (Shields et al., 2011; Wilson and Elliott, 2009; Welzel et al., 2019)... Concerns over the 87 potential impacts of OWF installations on local ecosystems further include collision risks, noise pollution, 88 electromagnetic field and the introduction of invasive species (Lloret et al., 2022; Bailey et al., 2014; Teilmann 89 and Carstensen, 2012; Watson et al., 2024). As the size and scale of OWF increases, the risk of significant 90 cumulative effects arising is also expected to increase (Brignon et al., 2022; Gușatu et al., 2021). The drivers and interdependencies of these large-scale processes are not yet well understood and the precise impact of scour 91 92 induced sediment transport on the marine environment remains uncertain, highlighting the need for 93 interdisciplinary research utilizing field data.

In order to gain a better understanding of the geophysical changes following the installation of OWFs and potential impacts on the marine environment arising from it, this study analyses the scour development at OWES as a first step. This study builds its analysis on field data, including high-resolution bathymetry scans from British OWFs, which have recently been made publicly available. This provides an opportunity to extend the understanding of scour evolution and its key drivers using a cross-regional dataset. A total of 460 monopiles were analyzed to obtain local scour depthsdepth and their spatial distribution in dependence of selected hydrodynamic and geological drivers.

101 Understanding scour development is a critical first step in assessing potential environmental impacts. It will help 102 determine whether OWES and entire OWFs contribute to regional sediment mobilization and provide a foundation 103 for future research into the long-term morphological footprint of OWF installations and their broader ecological 104 effects. To contribute to the overarching goal of reducing uncertainty in scour predictions wards the overall goal, 105 the paper focuses on advancing understanding of seour at OWES this study analyzes by analyzing field data from 460 monopiles across 9 OWFs, situated in diverse ocean regimes with current velocities from 0.54 m/s to 1.77 m/s 106 (99th quantilepercentile), significant wave heights from 1.5 m to 2.7 m (99th quantilepercentile), water depths 107 from 5 to 35 m and grain sizes ranging from cohesive sediment (51.54 µ#m) to medium gravel (19872µ-#m). The 108 109 spatial distribution and variability of relative scour depthsdepth across and within these OWFs are determined and 110 correlated with selected hydrodynamic and sedimentological parameters, using Principal Component Analysis 111 (PCA). This analysis aims to (1) identify universal drivers of scour across all sites, (2) assess sediment specific 112 trends by grain size (d_{50}) and (3) evaluate site specific variability at the level of three selected OWFs (Robin Rigg, 113 Lynn and Inner Dowsing and London Array). The site specific analysis in Section 3.5 assesses the robustness of the global correlations under local conditions and provides insight into how local conditions influence scour 114 behavior. Collectively Ultimately, the results of the study will helpthese efforts aim to decrease uncertainty in 115 116 relative scour depthsdepth prediction by assessing the contribution of the main drivers of scour development from 117 multivariable field data.

- 118 This paper is organized as follows: Section 2 describes the study area and methodology in which the methods used
- 119 to obtain the relative scour depthsdepth and selected on-site parameters are explained in detail (subsections 2.2 –
- 120 2.5). Additionally, the application of the Principal Component Analysis (PCA) to identify the primary correlation
- 121 between these parameters and scour development is explained (subsection 2.6). The results are presented in section
- 122 3, followed by implications for scour predictions for OWF (section 4), limitations and future research discussion
- 123 (section 54) and ending with the conclusions (section 65).

124 2 Study area and methodology

125 2.1 Study area

- 126 The research area, located in British waters, is illustrated in Figure 1, showing the specific locations of the nine
- 127 studied OWFs. Figure 1A provides a general overview, while Figure 1B pinpoints the positions of the OWFs,
- 128 labeled 1 to 9. These OWFs correspond to Robin Rigg, Barrow, Teesside, Humber Gateway, Lincs, Lynn and
- 129 Inner Dowsing, Greater Gabbard, London Array, and Gunfleet Sands-OWFs, respectively. Figures 1C and 1D
- display the 99th quantile percentiles of the significant wave heights $(H_{s,99})$ and current velocity magnitudes $(U_{99\epsilon})$
- 131 at the nine locations, respectively.
- 132 Notably, wind farms such as Robin Rigg and Barrow are situated in the Irish Sea, while the remaining seven are
- 133 located in the North Sea at the east coast of UK (Fig 1B). Water depths depth (h) ranging from 5 to 35 m can be
- 134 found across the nine OWFs. Depth data (h) were obtained from EMODNET
- 135 (https://emodnet.ec.europa.eu/en/bathymetry). The OWF located in the shallowest water depthsdepth is Robin
- 136 Rigg with h ranging from 1 to 14 m (Fig. 1B). Conversely, the OWF with the deepest water depths depth is Greater
- **137** Gabbard with *h* ranging from 21 to 35 m (Fig. 1B).
- 138 The highest and lowest significant wave heights (99th quantile percentile) can be found at Humber Gateway OWF
- 139 $(H_s = 2.7 \text{ m})$ (Fig. 1C-D) and at Gunfleet Sands OWF $(H_s = 1.5 \text{ m})$, which are located at the mouths of the Humber
- 140 and Thames estuaries (Fig. 1C-D), respectively. Regarding the quantile of current velocities, the highest value is
- 141 found at Robin Rigg OWF with 1.8 m/s (Fig. 1C-D), while the lowest value is found at Gunfleet Sands OWF with
- 142 a value of 0.4 m/s (Fig. 1C-D).
- 143 Depending on the locations of the OWFs, the seabed conditions vary from sandbanks featuring a variety of
- 144 bedforms to intertidal mudflats. Accordingly, the sediment also varies from silt to coarse and very coarse gravel,
- 145 with the sediment at Teesside OWF consisting of fine and silty sands and that at Humber Gateway consisting of
- 146 sandy gravel and boulders. In contrast, OWFs such as London Array and Greater Gabbard are located in the Outer
- 147 Thames Estuary with sandbanks and channels, while others such as Barrow and Robin Rigg have distinct
- 148 geological features such as megaripples, mudflats and deposits from different geological eras.

149 2.2 Data description

- 150 Bathymetric datasets from the nine OWFs considered in this study were collected via multibeam echosounder
- 151 (MBES) before, during and after the construction of the OWFs and were afterwards made available by its operators
- 152 via the Marine Data Exchange (MDE).
- 153 In total 460 OWES (of 680 available) with monopiles foundations were analyzed in this study. For the correlation
- 154 between scour and hydrodynamic conditions at the nine studied OWFs, metocean hindcast datasets (i.e., significant
- 155 wave height (H_s) and velocity magnitude $(U_{\overline{\epsilon}}U)$) by the Copernicus Marine Service (CMEMS)
- 156 (https://marine.copernicus.eu/) were used (CMEMS, 2023a, 2023b).

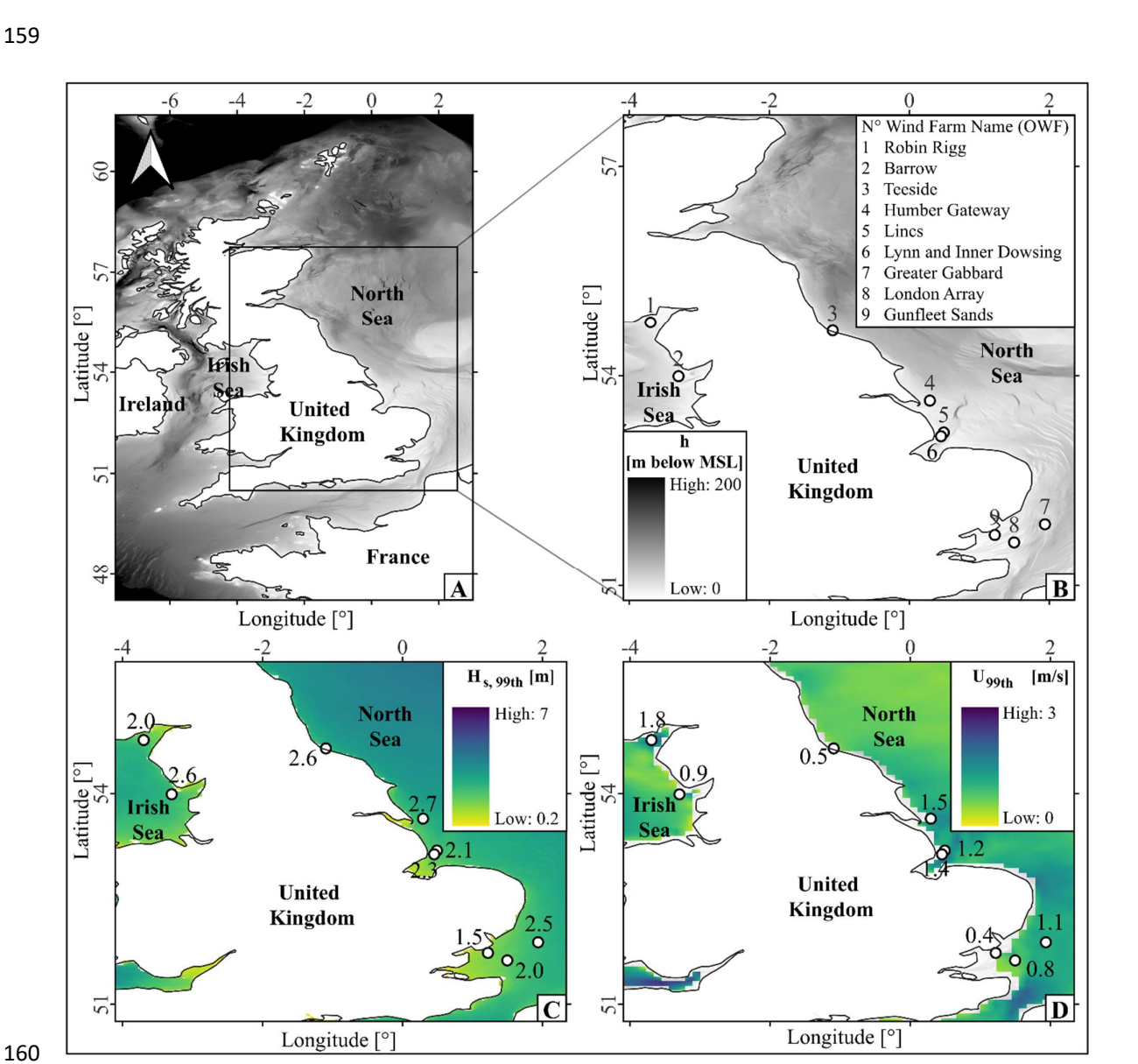


Figure 1: A) Study area. B) Location of the nine studied OWFs. Shown bathymetry data originates from EMODET (https://emodnet.ec.europa.eu/en/bathymetry). C) 99th quantilepercentile of significant wave heights (H_s) based on data for the year 2012. D) 99th quantilepercentile of current velocity magnitudes ($U_{\epsilon}U$) based on data for the year 2012.

Table 1 shows the OWFs considered in this study and provides an overview of their structural characteristics as 171 172 well as the hydrodynamic and geotechnical site conditions. Pile diameters (D) were obtained from Negro et al. 173 (2017), water depths (h) are based on EMODET (2020), dD_{50} represents the median grain diameter of the 174 sediment. The sediment data shown in Table 1 were obtained in Phi units from each OWF's benthic reports, then 175 converted to dP_{50} values in micrometers (μm) according to Bunte et al. (2001). The scour depth S represents the deepest scour at an individual OWES. The number of turbines OWES varies from 26 turbines OWES installed at 176 Teesside OWF to 174 turbines OWES installed at London Array OWF, indicating the different operational scales. 177 178 For some OWFs, including Lynn and Inner Dowsing, extensive bathymetric data spanning over ten years was 179 available. In contrast, others, such as Humber Gateway, had more limited bathymetric data with a coverage duration of four years. The highest grid resolutions of the bathymetric datasets found at each OWF varied from 180 181 0.2 to 0.5 m, with the highest resolution of the bathymetries found at each OWF being used. The earliest 182 bathymetry was collected at Barrow OWF in 2005 and the most recent was collected at Lynn and Inner Dowsing 183 in 2017, highlighting the long-term monitoring efforts at the wind farms. However, in this study only scour 184 depthsdepth obtained from the pre- and the first post-construction bathymetries were considered. The shortest 185 period between pre and post bathymetries was found at Lincs OWF with 377 days between August 2010 and 186 August 2011, while the longest period between scans was detected at Greater Gabbard OWF with 2902 days (~8 187 yrs) between June 2005 and May 2013. 188 Furthermore, environmental and hydrodynamic conditions associated with each OWF are also shown in Table 1, 189 which are essential for understanding how different variables contribute to scour around monopiles. These variables include the 99th quantile percentile significant wave height $(H_{S,99})$, representing the average height of the 190 191 highest third of waves. The wave height has a direct influence on the wave-induced current velocity near the seabed 192 and thus strongly determines the bed shear stresses and the formation of the vortex system around the OWES (Sumer & Fredsøe, 2002; Schendel et al., 2018). The 99th quantile percentile current velocity magnitude (U_{egg}) 193 indicates the resultant of eastward (u_0) and northward (v_0) -tidal flow components, those represent the depth-194 average velocity magnitude, whereas U_{crit} depicts the critical flow velocity for sediment entrainment. Their ratio, 195 the flow intensity $(U/U_{cr})_{99} U_e/U_{er}$, is a key parameter in describing the general sediment mobility and has a 196 197 large impact (h/D) influences the formation of the horseshoe vortex in such a way that the size of the horseshoe 198 vortex is reduced as the flow depth decreases, resulting in a reduction in the relative scour depths depth. At greater 199 relative water depths depth $h/D \ge 5$) the relative scour depths depth becomes almost independent of relative water 200 depth (Sumer and Fredsøe, 2002). 201 The Froude number $(Fr_{99}Fr)$ and pile Reynolds number $(Re_{99}Re)$ are used to characterize the flow conditions around the pile and their calculations are shown in table 2, Equations 2 and 3. The Froude number indicates whether 202 203 the flow is dominated by gravitational or inertial forces.— With increasing Froude number, stronger inertial forces 204 produce more pronounced pressure gradients at the upstream face of the monopile. Promoting early boundary layer 205 separation and enhances the strength of the horseshoe vortex system near the seabed, which increases local bed 206 shear stress and accelerates sediment erosion. As shown by Hu (2021), these dynamics are key in amplifying scour. 207 Similarly, Corvaro et al. (2015) found that higher Froude numbers lead to larger vortex structures and increased 208 bed shear stress, resulting in deeper equilibrium scour depth. On the other hand, pressure gradients at the pile increase, which affects the flow field in the vicinity of the pile and typically leads to larger scour depth. Tihc 209

210 Reynolds numbers provides information on whether the flow is laminar or turbulent, and determines the 211 characteristics of the vortex system around the pile. 212 Additionally, the Keulegan-Carpenter number (KC_{99}) , which is used to determine the relative influence of drag and inertia forces, the formation of vortices, and the potential for sediment transport (Sumer & Fredsøe, 2002). 213 The mobility parameter $(\theta_{99}/\theta_{cr})$ is considered a key controlling factor for scour, as it reflects the onset of sediment 214 215 motion under given flow conditions (Soulsby, 1997; Whitehouse et al., 2000). The calculation of those two parameters are shown in table 2, equation 9 and 20. The datasets were obtained between pre- and post- construction 216 bathymetries. The data was collected over a one-year period, prior to the post-construction bathymetry." 217 218 Dimensionless parameters as given in Table 1 were calculated based on the equations summarized in 219 Table 2.

OWF name	N° of OWES	Pile diameter D (m)		Scour depths depth S (m)	Water depths depth h (m)	D ₅₀ (μm)	Wave height $H_{s,99}$ (m)	Current Velocity $U_{e,99}$ (m/s)	scour	Relative water depthsde pth h/D	number	Reynolds number Re ₉₉ Re	Keulegan Carpenter number KC99	Mobility parameter θ_{99}/θ_{cr}	Flow intensity $(U/U_{cr})_{99}U$
Robin Rigg	60	4.3	Min Max	1.3 10	5 14	167 267	2.36 2.59	1.55 1.77	0.30 2.32	1.03 3.07	0.13 0.23	5.14x10 ⁶ 5.86x10 ⁶	<u>0.99</u> <u>1.9</u>	15.3 25.4	3.51 4.43
Barrow	30	4.75	Min Max	0.98 6	15 23	138 445	2.43 2.52	0.91 1.11	0.20 1.20	3.67 4.71	0.06 0.08	3.50x10 ⁶ 4.26x10 ⁶	<u>0.34</u> <u>0.48</u>	<u>4.4</u> <u>7.2</u>	1.89 2.40
Teesside	26	5	Min Max	0.65 1.62	8 20	51 166	2.52 2.76	0.54 0.54	0.13 0.32	208 3.49	0.04 0.05	2.10x10 ⁶ 2.10x10 ⁶	1.2 1.6	<u>6.1</u> <u>9.6</u>	1.19 1.29
Humber Gateway	72	4.2	Min Max	0.5 2.51	15 20	5918 1900 0	2.24 2.37	1.51 1.56	0.11 0.59	3.65 4.65	0.11 0.12	4.87x10 ⁶ 5.06x10 ⁶	0.92 1.11	<u>0.4</u> <u>1.2</u>	0.58 0.99
Lincs	75	5.2	Min Max	0.54 1.92	12 21	505 1982	2.47 2.71	1.07 1.67	0.10 0.38	2.41 3.88	0.08 0.13	4.29x10 ⁶ 6.71x10 ⁶	0.64 1.01	2.6 11.1	1.31 3.12
Lynn and Inner Dowsing	60	4.74	Min Max	0.5 2.35	9 17	684 1950	2.11 2.36	1.30 1.45	0.10 0.49	2.10 3.47	0.11 0.13	4.76x10 ⁶ 5.29x10 ⁶	0.84 1.3	3.2 7.3	1.63 2.53
Greater Gabbard	139	6	Min Max	0.5 4.54	23 35	394 2296	2.41 2.67	1.02 1.22	0.08 0.75	3.50 5.83	0.05 0.07	4.72x10 ⁶ 5.64x10 ⁶	$\frac{0.18}{0.33}$	1.3 6.1	1.14 2.25
London Array	174	7	Min Max	1.2 9.5	1 27	120 930	1.89 2.36	0.71 0.81	0.21 2.02	0.31 4.67	0.04 0.19	2.56x10 ⁶ 3.56x10 ⁶	<u>0.1</u> <u>2.3</u>	1.5 32.6	1.14 2.33
Gun <mark>d</mark> fleet Sands	49	4.7	Min Max	0.88 7.73	2 16	146 253	1.52 1.72	0.48 0.86	0.18 1.64	0.54 3.34	0.03 0.09	1.74x10 ⁶ 3.12x10 ⁶	<u>0.45</u> <u>1.68</u>	<u>2.1</u> <u>17.6</u>	1.05 2.07

Table 1. Overview of studied OWFs with hydrodynamic and sedimentological site conditions.

Variable	Equation	
Current velocity	$U_{e,99} = \sqrt{u_0^2 + v_0^2}$	(1)
Froude number	$Fr_{99}Fr = rac{U_e}{\sqrt{gh}}$	(2)
Pile Reynolds number	$Re_{99}Re = \frac{U_{e,99}D}{v}$	(3)
Relative density	$s = \frac{\rho_s}{\rho_w}$	(4)
Relative Dimensionless grain size	$D_* = \left(\frac{\rho g}{v^2}\right)^{\frac{1}{3}} d \underline{\mathcal{P}}_{50}$	(54)
Critical Shields	$\theta_{cr} = \frac{0.3}{1 + 1.2D_*} + 0.55(1 - \exp(-0.02D_*)$	(6 <u>5</u>)
U_{cr}	$U_{cr} = 7 * \left(\frac{h}{dD_{50}}\right)^{\frac{1}{7}} (g(s-1)dD_{50}\theta_{cr})^{0.5}$	(7 <u>6</u>)
Flow intensity	$(\frac{U}{U_{cr}})_{99}\frac{U_{e,99}}{U_{er}}$	(8 7)
Zero crossing period (T_z)	$\frac{T_p}{1.28}$	<u>(8a)</u>
Natural period (T_n)	$T_n = \sqrt{rac{h}{g}}$	<u>(8b)</u>
A_{t}	$A_t = (6500 + \left(0.56 + 15.54 \frac{T_n}{T_z}\right)^6)^{1/6}$	<u>(8c)</u>
RMS velocity (U _{rms})	$A_{t} = (6500 + \left(0.56 + 15.54 \frac{T_{n}}{T_{z}}\right)^{6})^{1/6}$ $U_{rms} = 0.25 \frac{H}{T_{n}(1 + \left(A_{t} \frac{T_{n}^{2}}{T_{z}}\right))^{3}}$	<u>(8d)</u>
Wave-induced velocity (U _m)	$U_m = \sqrt{2} \ U_{rms}$	<u>(8e)</u>
<u>Keulegan-Carpenter</u> <u>number (KC)</u>	$KC_{99} = \frac{U_m T_p}{D}$	<u>(9)</u>
Roughness related to d_{50} (ks)	$k_s = 2.5d_{50}$	<u>(10)</u>
Amplitud of wave orbital motion at the bed (A)	$A = \frac{U_m T_p}{2\pi}$	<u>(11)</u>

228 The values assumed for all OWFs sites are:

229 $\rho_s = 2650 \, kg/m^3 \, \rho_w = 1027 \, kg/m^3 \, v = 1.3x 10^{-6} m^2/s \, g = 9.8 \, m/s^2$

Where ρ_s is the sediment density, based on Soulsby (1997). ρ_w is the water density, v is the kinematic viscosity

and g the gravitational acceleration. Equation 4 was calculated based on van Rijn (1984), where D_{*} is the non-

232 dimensional grain diameter that is used to calculate the critical Shields parameter (θ_{cr}), which represents the

233 threshold for initiation of motion at the bed, as proposed by Soulsby (1997).

Equation 5 is taken from Soulsby and Whitehouse (1997), where $s(s = \rho_s/\rho_w)$ represents the specific gravity of

235 sediment grains. The d_{50} represents the median sediment grain size.

236 In equation 18, the maximum bed shear-stress value (τ_{max}) was calculated following Roulund et al. (2016), which

237 <u>builds upon Soulsby (1997) by combining current- and wave-induced shear stress through a directional correction.</u>

238 Shields parameter (θ_{99}) is derived using equation 19, based on the maximum bed shear stress (τ_{max}) under

239 combined wave and current conditions. The Keulegan-Carpenter number is defined in equation 10, where T_p is

240 the peak wave period and D the monopile diameter.

241 Equation 20 provides the calculation of the mobility parameter to assess sediment mobility, providing a

242 dimensionless indicator of whether the hydrodynamic forcing was sufficient to initiate sediment motion. All

243 relevant equations are summarized in table 2.

Sediment density $(\rho_{\rm x})$ is 2650 kg/m³, a value assumed for all OWFs sites based on Soulsby (1997). The water 245 246 density (ρ_{uv}) , which represents sea water at the surface, is 1027 kg/m^3 . The kinematic viscosity (v) is $1.3e-6 \text{ m}^2/\text{s}^2$, and the gravitational acceleration (g) is 9.8 m/s². Equations 4 and 6 are 6 is taken from Soulsby and Whitehouse 247 (1997), where $s (s = \frac{\rho_s}{\rho_{sa}})$ represents the specific gravity of sediment grains, in addition introduce here d50. 248 249 Equation 5 4 was calculated based on van Rijn (1984), where D_{*} is the non-dimensional grain diameter, and this is first calculated to calculate the critical Shields parameter (θ_{ex}) Soulsby and Whitehouse (1991) introduced the 250 expression for the critical Shield parameter, which corresponds to the initiation of motion at the bed. The 251 northward (v_0) and eastward (u_0) current velocities in the water column in a temporal resolution of 1 hour are 252 253 used to calculate the U_{c-99} .

254255

256

257258

259260

- In addition, the minimum and maximum values of the variables at each OWF are shown. The 99th quantilepercentile of significant wave heights ($H_{s,99}$) in a temporal resolution of 3 hours and current velocities ($U_{c,99}$) in a time window of 1 hour are used in this study. The 99th quantilepercentile was chosen for this study, due to scour development being more driven by largest $H_{s,99}$ and $U_{c,99}$. 1990The datasets were obtained between pre—and post—construction bathymetries. The data were collected over a one year period, prior to the post-construction bathymetry.
- Since some hydrodynamic parameters (e.g. wave period or orbital flow velocity) and geotechnical data (e.g. grain density and size distribution) were not directly available for all locations during the preparation of this study, it was not possible to determine other dimensionless parameters (Shields, KC, Ucw) that are important for the scour process with sufficient reliability.

265 2.3 Pre-processing of bathymetric data

266 Figure 2 shows the workflow used in this study, starting with the acquisition of bathymetric datasets, originally obtained from the Marine Data Exchange, and their conversion to Ordnance Datum Newlyn (ODN). This was 267 268 followed by the generation of 100m x 100m tiles for each available bathymetric dataset, centered on each turbine 269 location. If bathymetric scans with different spatial resolutions were available for the same date, only the one with 270 the highest resolution was used. In addition, some turbine locations could not be further analysed due to missing 271 pre-construction scans or poor data quality. Tiles with more than 50% empty cells were discarded because a high 272 percentage of missing data increases the likelihood that important areas, such as the scour region, are poorly 273 captured. Tests were conducted with lower missing cell thresholds (10% and 25%), but even with 50% missing data, valuable information for scour analysis was retained. Using a stricter 25% threshold, too many tiles were 274 275 lost, including those that still contained useful data. As a result, 460 of the 680 turbines OWES across in the nine 276 OWFs were analyzed in more detail in this study.

The difference in bed elevation at turbine sites between the pre-construction (Fig 2.A) and post-construction surveys (Fig 2.B), was used for extracting scour information. The deepest scour at each turbine site was then extracted from the difference plot (Figure 2.C). A detailed description of this part of the workflow is provided in the next chapter section 2.4.

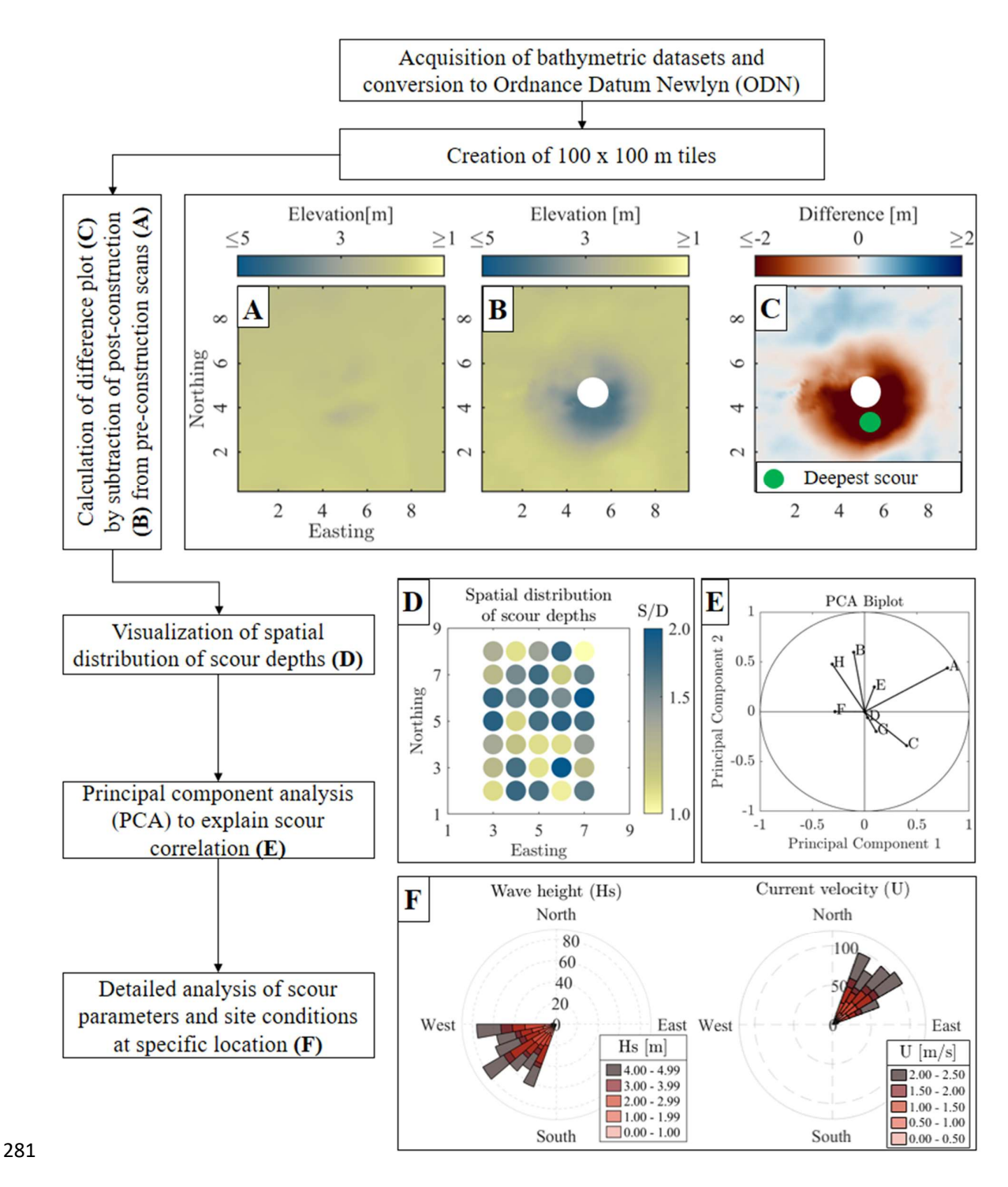


Figure 2: General workflow and methodology used to assess the scour distribution and evolution as well as the correlation between scour parameters and site conditions. A) Pre-installation scan. B) Post-installation scan. C) Difference plot after subtraction of B from –A. D) Map of spatial distribution of <u>relative</u> scour <u>depthsdepth (S/D)</u>. E) Principal Component Analysis (PCA). F) Site conditions of wave heights and current velocities.

2.4 Calculation of scour parameters

- 288 First, to eliminate outliers, a threshold based on the 99th percentile was used to filter out extreme values, ensuring
- 289 that outliers did not skew subsequent analyses or visualizations. Subsequently, to address potential offsets between
- 290 pre- and post-construction, a median filter was applied to both datasets. The difference in medians, excluding the
- 291 presumed scour area, was considered the offset. This offset was then applied while calculating the difference plot
- 292 between the pre- and post-construction bathymetries (Fig. 2A-C). To remove additional outliers close to the
- 293 turbine, an area equivalent to 110% of the pile's foodprint footprint area was excluded from the center of the
- 294 difference plot.
- 295 The deepest scour depth (see green dot in Fig. 2C) was then extracted from the difference plot (Fig. 2C). The
- 296 calculated relative scour depths were then visualized to show the spatial distribution across the nine OWFs (Fig.
- 297 2D).

298 2.5 Principal component analysis (PCA)

- 299 In the case of field data, the correlation of the scour process with hydrodynamic and geotechnical variables is
- 300 complicated by the simultaneous change of several of these variables. In order to reduce the complexity and
- 301 simplify this multivariate problem, PCA was used in a next step (Fig. 2.E). PCA works by transforming the data
- 302 into a set of new variables called principal components, which are linear combinations of the original variables
- 303 (Jolliffe & Cadima, 2016). These components are ordered based on how much variance they explain, with the first
- 304 principal component (PC1) explaining the maximum variance in the data, followed by the second principal
- 305 component (PC2). Each component also has an eigenvalue, which shows the amount of variation it captures.
- 306 Generally, the PCA is able to handle lots of independent variables and helps to simplify the data without losing
- 307 important information (Harasti, 2022). Unlike studies that use PCA for variable reduction (Harasti, 2022), in our
- 308 analysis we retained all principal components to identify and quantify the relationships between the selected
- 309 variables.
- 310 In this study, the PCA was applied to a dataset of 692 turbines OWES, including 460 from our analysis and an
- 311 additional 177 turbines232 OWES from London Array OWF-and 100 turbinesOWES from Thanet OWF, based
- 312 on Melling's (2015) data. The PCA was then performed using eight independent variables that contributed to the
- 313 principal components. Those dimensionless variables were the relative water depths depth (h/D), wave height
- 314 $(H_{s,99})$, current velocity $(U_{c,99})$, Keulegan-Carpenter number (KC_{99}) , mobility parameter $(\theta_{99}/\theta_{cr})$, Reynolds
- 315 number $(Re_{99}Re)$, Froude number $(Fr_{99}Fr)$, relative sediment size $(D/d_{50}D_{50})$, flow intensity $((U/U_{Cr})_{99}U_{e,99}/U_{e,99})$
- 316 U_{ex}), and the relative scour depths depth (S/D). Following this, the data was organized into a matrix, with each row
- 317 representing a specific OWES and each column representing a selected dimensionless variable. All the variables
- 318 were extracted as representative values specific to the OWES, with the focus on the 99th percentile to capture
- 319 extreme hydrodynamic conditions. Scour processes are more likely to occur in these extreme conditions because
- 320 maximum scour depth usually develops during storm-induced events, rather than under mean or median values.
- 321 Subsequently, the variables were standarized to ensure the comparability of the results.
- 322 All the variables were extracted as representative values specific to the OWES, such as the 99th percentile and
- 323 standardized to ensure comparability.
- 324 In some studies, the PCA is used for reducing the number of dimensions (Harasti, 2022), or to help develop
- 325 predictive models grouped by soil classes (Annad, 2023). However, the aim of this study was to keep all the

principal components. This approach enabled the full exploration of the interdependence between physical drivers 326 327 and scour response across sites. To interpret the relationships among the variables, a principal component analysis 328 biplot was generated (Gabriel et al., 1971). In the biplot, variables are represented as vectors, and the angle between vectors indicates the degree of correlation. The strength of the correlation was quantified using the cosine of the 329 angle (Jolliffe & Cadima, 2016), enabling us to assess the strength of association between each variable and scour 330 331 variability (S/D) across different OWFs sites. Similar to previous studies that applied PCA for parameter selection 332 in bridge pier or scour formula development (Harasti, 2022; Annad, 2023), this multivariate analysis provides a 333 clearer understanding of which parameters dominate the scour process under real offshore conditions

334

- In order to correlate the relative scour depths (*S/D*) with the other variables, the PCA biplot (Fig. 4) was employed to estimate the correlation between the variables (Gabriel et. al., 1971). In the biplot (Fig. 4), the angle between the respective vectors indicates the degree of correlation, with an angle close to 0° indicating a strong positive correlation, while 180° indicates a strong negative correlation and 90° indicates no correlation at all. Each correlation percentage was thus calculated by taking the cosine of the measured angle between vectors, thereby providing an estimation of how closely variables within the analysed dataset are related the relative scour depths (S/D).
- An additional approach to reducing the complexity of multivariate datasets is to initially group the data based on a selected key variable. Accordingly, the PCA was also applied to the dataset after it had been grouped by grain size (dD_{50} diameter) classes (Annad et al., 2021), given that the sediment characteristics of the seabed play a significant role in local scour (Qi et al., 2016). This approach facilitated a more precise estimation of local scour, thereby reducing uncertainties related to sediment.

347 3 Results

348 3.1 Spatial distribution of relative scour depthsdepth

- 349 To illustrate the variability in relative scour depths depth between the nine studied OWFs and within single OWFs, Figure 3 shows the spatial distribution of relative scour depths depth. There are clear differences between OWFs 350 in both the magnitude and variability of relative scour depthsdepth. For example, at OWF Robin Rigg (Figure 351 352 3.A), the highest relative scour depthsdepth were identified, the values range from 0.29–S/D=0.29 to -2.49S/D=2.49. This OWF is characterized by fine and medium sands. In contrast, the smallest relative scour 353 354 depthsdepth occurred at the OWF of Lines and Lynn and Inner Dowsing (Figure 3.E and 3.F), with values from 355 0.12–S/D=0.12 to 0.92–S/D=0.92, which is possibly linked to -coarse sands presented at both-this sites-. Furthermore, the highest variability ($\sigma = 0.44$) in relative scour depths depth were detected at OWF London Array 356 357 (Figure 3.H) and Barrow (Figure 3.B), likely influenced by the complex seabed morphologies and sediment 358 compositions in these areas. On the other hand, the significant variability at London Array may be explained by 359 the presence of the Long Sand and Kentish Knock sandbank. This illustrates how different site characteristics can result in various scour distributions, even within a single OWF. 360
- The remaining OWFs showed relatively low <u>relative</u> scour <u>depthsdepth</u> and little spatial variability, even though site conditions were significantly different, as indicated by their seabed conditions from very fine sand for Teesside (Figure 3.C) to coarse and very coarse gravel for Humber Gateway (Figure 3. D).

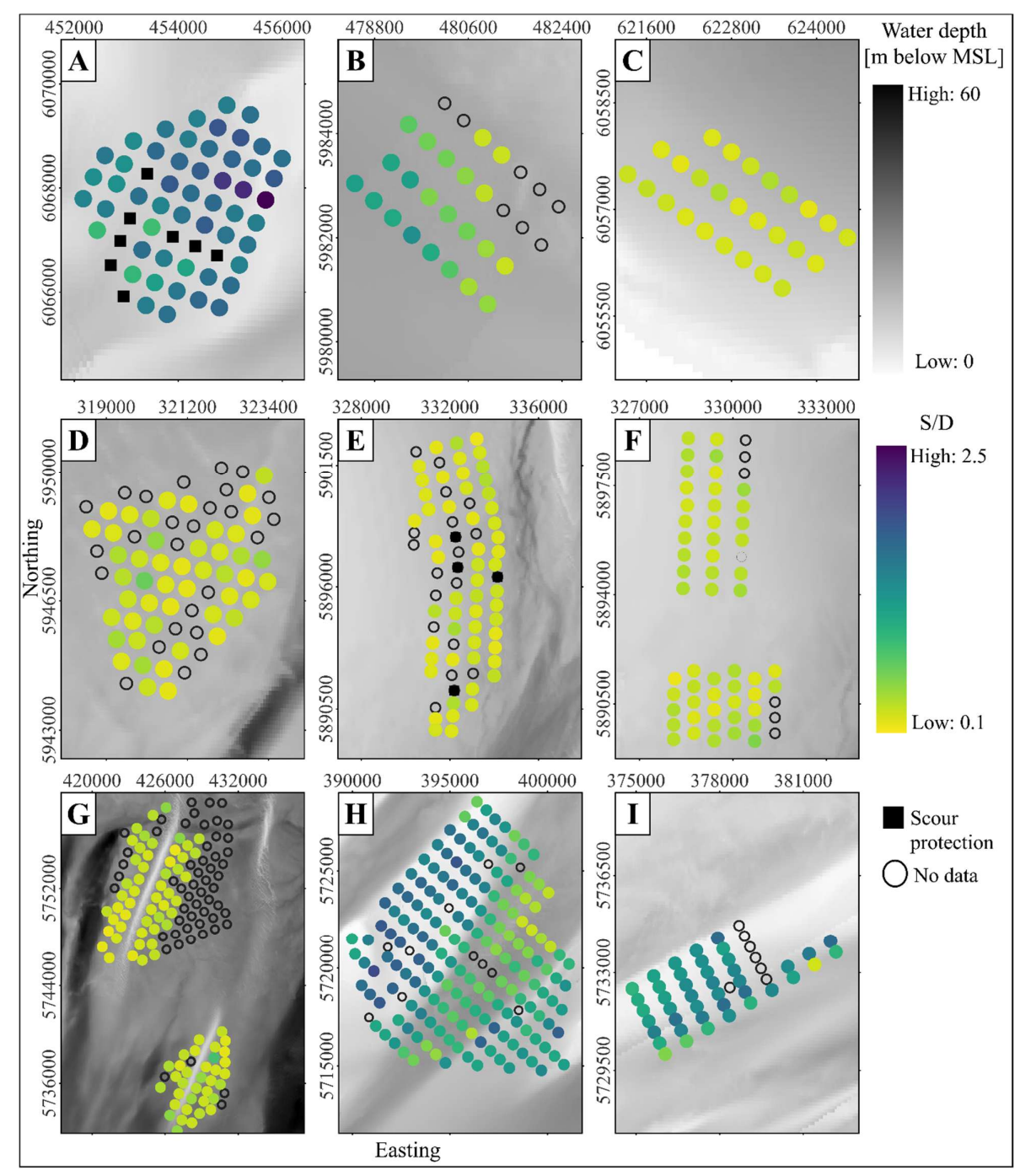
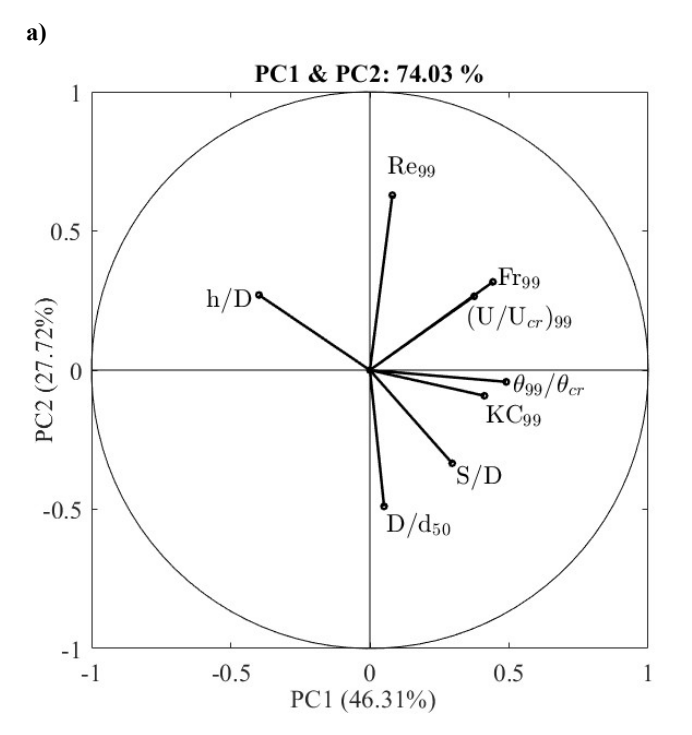


Figure 3: Spatial distribution of relative scour depthsdepth-(S/D) at the nine studied OWFs. Numbered Letterred markers (A1_91) denote the locations of Robin Rigg, Barrow, Teesside, Humber Gateway, Lincs, Lynn and Inner Dowsing, Greater Gabbard, London Array, and Gunfleet Sands OWFs, respectively. The upper colorbar represents water depthsdepth, with darker shades indicating deeper water. The lower colormap indicates relative scour depthsdepth, with darker blue color indicating largest scour. Black filled squares represent turbinesOWES with scour protection, while empty circles denote missing data. Shown bathymetry data originates from EMODET (59).https://emodnet.ec.europa.eu/en/bathymetry).

3.2 Principal component analysis (PCA)

The analysis of Figure 3 reveals notable variations in <u>relative</u> scour <u>depthsdepth</u> across individual OWFs. This variance underscores the need for a more detailed examination of specific wind farm characteristics to identify the drivers of scour. To this end, a PCA was conducted to correlate <u>relative</u> scour <u>depthsdepth</u> and selected parameters by identifying and quantifying their relationships. The PCA biplot presented in Figure 4 illustrates these correlations between <u>relative</u> scour <u>depthsdepth</u> and the studied variables and provides a comprehensive view of how different factors interact and influence <u>relative</u> scour <u>depthsdepth</u>.

b)



Variables	θ to S/D	%Cosine-
		based
		Correlation
		with S/D
$h/D_{\overline{D}_{50}}$	<u>165.59</u> 171.49	0.989 <u>0.96</u>
$D/d_{50}h/D$	<u>35.53</u> 171.053	0.988 <u>0.81</u>
$KC_{99}H_{\overline{s,99}}$	<u>35.91</u> 149.91	0.865 <u>0.80</u>
θ_{99}/θ_{cr} Fr	<u>43.60</u> 61.9	0.469 <u>0.72</u>
Re ₉₉ Re	<u>131.21</u> 117.2	<u>0.456</u> <u>0.65</u>
$(\frac{U}{U_{cr}})_{99} \frac{U_{c,99}}{U_{c,99}}$		
/U_cr	<u>83.84</u> 63.0	0.453 <u>0.11</u>
$Fr_{99}U_{c,99}$	106.8 <u>84.17</u>	<u>0.289</u> <u>0.10</u>

Figure 4: a) PCA biplot, illustrating the correlation between variables and relative scour depthsdepth (S/D).

b) The table detailing the angles between the relative scour depth S/D and the other variables (in degrees),

along with the magnitude cosine-based correlation (values from 0 to 1), where values closer to 1 indicates

stronger correlation, as well as their corresponding percentage correlation.

As shown in the biplot, PC1 and PC2 account for 74.0382% of the variation in the data set. This high percentage indicates that these two components capture most of the significant patterns in the data, allowing for a meaningful interpretation of the relationships among the variables. In the biplot, each vector stands for a variable, with the direction and magnitude of the vector reflecting its contribution to the principal components—. The variables that contribute the most to the variance in PC1 are the mobility parameter, the Froude number, and Keulegan Carpenter number, with shares of 0.4898, 0.4419, and 0.4114, respectively. In contrast, the variance in PC2 is primarily explained by the pile Reynolds number, the relative grain size and the Froude number, with shares of 0.628, - 0.489, and 0.3168, respectively. This significant contribution of the mobility parameter, the Froude number, and the Keulegan Carpenter number to PC1 suggests that variations in these hydrodynamic parameters are critical in shaping the principal dynamics of the dataset. The variables that contribute the most to the variance in PC1 are flow velocity ($U_{e,99}$) and Reynolds number (Re), with loadings of 0.5303 and 0.5248, respectively. In contrast, the variance in PC2 is primarily explained by the relative water depths (h/D) and the relative scour depths (h/D), with loadings of 0.548 and 0.49732, respectively. This significant contribution of flow velocity (h/D) and Reynolds

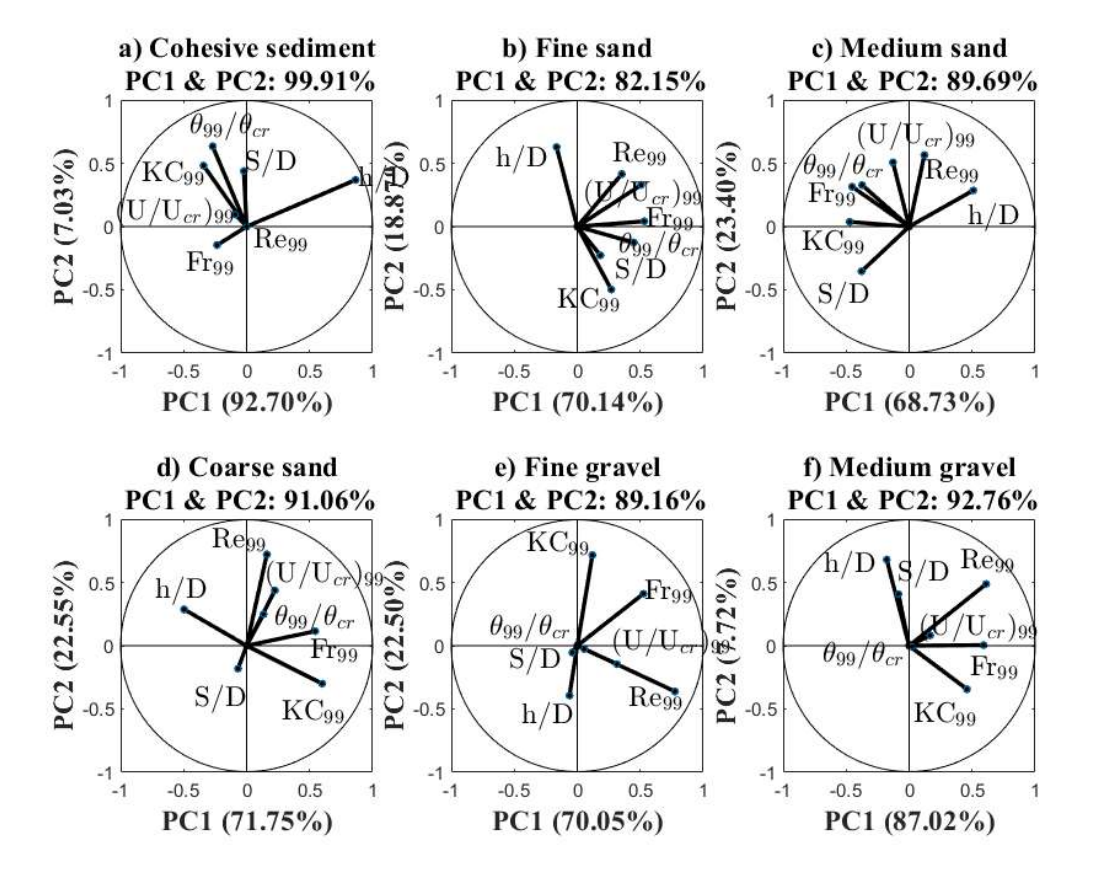
396 number (Re) to PC1 suggests that variations in these hydrodynamic parameters are critical in shaping the principal dynamics of the dataset. 397 398 The table (Fig. 4b) next to the biplot provides further insight by showing the angular distances between the S/D399 vector and each of the other variables, as well as their respective correlation coefficients. One of the key 400 observations is that relative scour depth has the strongest negative correlation of 0.96 with the relative water depth, 401 which underscores the critical role of water depth in governing scour intensity. Shallower relative depths 402 concentrate flow energy at the bed, intensifying near-bed velocities and shear stresses that promote deeper scour holes (Smith & McLean, 1977; Whitehouse, 2010). The next strongest correlation is with the relative grain size 403 with a correlation factor of 0.81. This suggests that as the relative grain size increases, relative scour depth also 404 tends to increase. This trend is in line with the functional dependence of relative scour depth on relative grain size 405 as observed by Sheppard et al. (1995, 1999). This positive trend may be due to increased turbulence caused by 406 407 larger bed roughness elements or the initiation of larger-scale scour processes around coarser particles under 408 certain flow conditions (Whitehouse, 2010). 409 Furthermore, a significant positive correlation was found with the Keulegan-Carpenter number with a correlation 410 factor of 0.81, indicating the importance of oscillatory flow conditions in scour development. Higher Keulegan 411 Carpenter number directly leads to higher relative scour depth (Sumer and Fredsoe, 2002). This is driven by the onset of the horseshoe vortex and lee-wake eddy shedding (Sumer et al., 1992b; Zanke et al., 2011), with increased 412 permanence of the horseshoe vortex and amplification of bed shear stresses at higher KC values (Sumer et al., 413 1997). In addition, the mobility parameter exhibits a strong positive correlation (0.71) with the relative scour depth. 414 415 The mobility parameter quantifies the instantaneous capacity of the flow to exceed the entrainment threshold, 416 driving rapid sediment entrainment when significantly above unity (Soulsby, 1997; van Rijn, 1993). Variables 417 such as the pile Reynolds number, the flow intensity, and the Froude number, although less correlated with relative 418 scour depth, contribute more to the total variance. This suggests that these flow-related variables influence relative 419 scour depth through more complex or non-linear interactions with other hydrodynamic conditions and sediment 420 characteristics. 421 Since seabed sediment characteristics play a significant role to local scour (Qi et al., 2016), the PCA was applied again to the same dataset but pre-clustered into different soil classes (Annad et al. 2021). By reducing the 422 423 uncertainties related to grain size (d_{50}) , this analysis should provide a better estimation of the local scour. This 424 classification also facilitates the identification of parameters that are more influential in estimating scour for 425 specific soil classes rather than uniformly across different types. After the clustering, six soil classes were obtained: 426 cohesive sediment $(d_{50} \le 63 \mu m)$ with 5 data points, fine sand $(63 \le d_{50} < -200 \mu m)$ with 203 data points, medium $\underline{\text{sand } (200 \le d_{50} \le -630 \ \mu m) \text{ with 249 data points, coarse sand } (630 \le d_{50} \le -2000 \ \mu m) \text{ with 170 data points,}}$ 427 428 <u>fine gravel (2000</u> $\leq d_{50} < -6300 \ \mu m$) with 18 data points, and medium gravel ($d_{50} \geq -6300 \ \mu m$) with 49 data 429 points. 430 The table (Fig. 4b) next to the biplot provides further insight by showing the angular distances between the S/D vector and each of the other variables, as well as their respective correlation coefficients. One of the key 431 observations is that despite its relatively small contribution to the total variance (as indicated by the shorter vector length in the biplot), sediment size (D_{50}) has the strongest negative correlation with scour depths (S/D), as

indicated by a correlation coefficient of 0.989. This highlights the critical influence of sediment size on scour 434 processes, even though it does not account for much of the variance captured by the first two principal components.

This observation can be explained by the underlying physical processes that affect scour depths. As noted by 436 Whitehouse (2010) for non-cohesive sediments, larger sediment sizes are more resistant to erosion, resulting in 437 438 reduced scour depths. Therefore, while D_{sn} is strongly correlated with scour depths, it does not explain the broader variability in the data that is influenced by other factors. Variables such as flow velocity $(U_{e,99})$, Reynolds number 439 440 (Re), and Froude number (Fr), although less correlated with scour depths, contribute more to the total variance. This suggests that these flow related variables influence scour depths through more complex or non-linear 441 interactions with other hydrodynamic conditions and sediment characteristics. 442

Given that the initial PCA analysis indicates the strongest negative correlation between $dD_{\Sigma\Omega}$ and S/D, a more indepths investigation of the influence of D_{50} on scour processes is required. Since the sediment characteristic of the seabed plays a significant role to local scour (Qi et al., 2016), the PCA was applied to the same data set, but preclustered into different soil classes (Annad et al., 2021). By reducing the uncertainties related to sediment size, this analysis should provide a better estimation of the local scour. This classification also facilitates the identification of parameters that are more influential in estimating scour for specific soil classes rather than uniformly across different types.

3.3 Principal component analysis (PCA) by clustered soil classes 450



435

443

444 445

446

447

```
452
       Figure 5: PCA correlation by clustered soil classes based in the grain size (d_{50}), -classes remaining
       parameters that are shown in the biplots are explain in data description (section 2.2) between the remaining
453
       7 dimensionless parameters, including the secur depth. a) Cohesive sediment (d\mathcal{D}_{50} \leq 63 \ \mu m). b) Fine sand
454
       (63 \le d_{50} < 200 \mu m_{63} = 200 \mu m_{63}. c) Medium sand (200 \le d_{50} < 630 \mu m_{20} = 630 \mu m_{20}. d) Coarse sand
455
       (\underline{630} \le d_{50} < \underline{2000} \mu m \underline{630} \text{ to } \underline{2000} \mu m). e) Fine gravel (\underline{2000} \le d_{50} < \underline{6300} \mu m \underline{2000} \text{ to } \underline{6300} \mu m). f) Medium
456
       gravel (d_{50} \ge 6300 \, \mu m \frac{6300 \text{ to } 20000 \, \mu m}{20000 \, \mu m}). Clustering of the grain size (dD_{50}) was based on Annad et. al.
457
458
       (2021).
459
       Building on the initial PCA analysis, which emphasized the significant influence of grain size (D_{50}) on relative
460
       scour depthsdepth (S/D), a more detailed investigation was conducted by categorizing the dataset into six grain
       sizesoil classes: cohesive sediment (d_{50} \le \underline{63} \mu m D_{50} \le \underline{63} \mu m) with 5 data points, fine sand (\underline{63} \le d_{50} < \underline{200})
461
       \mu m63 \text{ to } 200 \ \mu m) with 203 data points, medium sand (\underline{200} \le d_{50} < \underline{630} \ \mu m200 \text{ to } 630 \ \mu m) with 2\underline{4906} data
462
       points, coarse sand (\underline{630} \le d_{50} < \underline{2000} \mu m 630 \text{ to } \underline{2000} \mu m) with \underline{170221} data points, fine gravel (\underline{2000} \le d_{50} < \underline{2000} \mu m)
463
464
       6300 \, \mu m \frac{2000 \text{ to } 6300 \, \mu m}{2000 \text{ to } 6300 \, \mu m}) with \frac{19 \cdot 18}{2000 \, \mu m} data points, and medium gravel (d_{50} \geq 6300 \, \mu m \frac{6300 \, \text{ to } 20000 \, \mu m}{20000 \, \text{ to } 20000 \, \mu m}) with
465
       4973 data points.
466
       Figure 5 shows PCA biplots for each soil class illustrating the relationships between relative scour depthsdepth
       the relative water depth, the Keulegan-Carpenter number, the mobility parameter, the pile Reynolds number, the
467
       flow intensity and the Froude number. The first two principal components (PC1 and PC2) explain between 82.15
468
469
       % and 99.91%
470
       (S/D) and the variables h/D, H_{S,99}, U_{c,99}, U, Fr, Re, and U_{c,99}, (U/U_{cr}). The first two principal components (PC1)
       and PC2) explain between 90.98% and 99.55% of the variance within each class, thus describing more of the
471
       variance in comparison to when the PCA was applied to all data. Data complexity seems to be greatly reduced by
472
473
       just removing the effect of sediment. In the cohesive sediment soil class (Figure 5a), relative scour depth is
474
       positively correlated with the mobility parameter. However, the calculation of the mobility parameter might
475
       contain larger uncertainties for cohesive soils (Soulsby, 1997), so the results should be treated with caution.
476
       In contrast, relative water depth has a strong negative correlation with relative scour depth in fine sand (Figure 5b)
477
       and medium sand (Figure 5c). This indicates that as relative water depth increases, relative scour depth tends to
478
       decrease in these finer soil classes. From a physical view, Melling (2015) found out that in similar substrates,
479
       relative scour depth agree well between different geographic locations and showed that OWES located in sandy
480
       sediments exhibit a strong influence of relative water depth on scour, suggesting geotechnical factors are less
481
       influential in coarser sediments. Although the observation that relative scour depth decreases as relative water
       depth increases might initially seem counterintuitive. This behavior is best explained through the transition
482
483
       between shallow-water and deep-water flow regimes. As flow approaches a pile, stagnation pressure develops on
       its upstream face, causing the flow to separate into an up-flow and a down-flow component. The down-flow is
484
485
       directed toward the bed and promotes the formation of a horseshoe vortex. Flow separation occurs at the stagnation
486
       point, defined as the location of maximum energy from the approaching flow at the pile face. The energy of the
487
       approach flow consists of hydrostatic and kinetic components, whose vertical distribution is governed by the
488
       boundary layer. In shallow water, the kinetic component dominates over hydrostatic pressure, resulting in a
489
       stagnation point located higher up the pile, near the water surface. This enhances down-flow and vortex activity,
```

with higher velocity gradients near the seabed, potentially leading to greater bed shear stresses and increased 491 sediment mobility. In contrast, in deeper water, hydrostatic pressure becomes more influential, leading to a more 492 493 uniform pressure field across the pile face and shifting the stagnation point closer to the bed. This results in weaker down-flow and reduced vortex strength, thereby diminishing the scour depth (FHWA, 2012; Harris & Whitehouse, 494 2014). Furthermore, Link and Zanke (2004) observed that maximum relative scour depth tends to develop more 495 496 slowly and reach lower values in deeper water depth, even under constant average flow velocity, due to reduced 497 shear velocity over the undisturbed bed. This highlights that the relationship between relative water depth and 498 scour is not necessarily linear. 499 The dynamics observed in coarse sand (Figure 5d) and fine gravel (Figure 5e) are different from the finer sediments. In these classes, the flow intensity and the Froude number show significant negative correlations with 500 relative scour depth, indicating that higher values of these parameters correspond to reduced relative scour depth. 501 502 However, these soil classes are also characterized by comparatively small relative scour depth, which makes the 503 relationship less prominent. sediment class (Figure 5a), PC1 dominates, explaining the majority of the variance, suggesting a primary 504 505 underlying pattern that drives the variability in scour depths. However, this result must be interpreted with caution 506 as the analysis in this group is based on only 5 data points. In contrast, the fine sand (Figure 5b) and medium sand (Figure 5c) classes show a more balanced contribution from PC1 and PC2. 507 508 Analysis of the correlations between scour depths (S/D) and other variables within each soil class reveals different 509 patterns. In the cohesive sediment class $(D_{\Sigma\Omega} \le 63 \ \mu m)$, relative scour depths is positively correlated with flow intensity $(U_{e,qq}/U_{ex})$. This suggests that as flow intensity increases, scour depths tends to increase, which meets physical expectations in clear water conditions, i.e. stronger flow intensity leading to larger scour (Melville, 2008). 511 512 However, the data points in this cluster belong to the Teeside OWF, for which flow intensities $(U_{c.99}/U_{cF})$ between 1.17 and 1.28 m/s were determined and thus live bed flow conditions. In contrast to clear water conditions, the 513 scour depths under live bed conditions are influenced by the migration of bed forms, typically leading to scour 514 515 depths smaller than that in clear-water conditions. It is important to note that the flow intensity vector $(U_{c,99}/U_{cr})$ 516 is remarkably short, reflecting its minimal contribution to the overall variability, despite its positive correlation with scour depths (S/D). Although $U_{e,pg}/U_{ex}$ is positively correlated with scour depths, its limited impact on the 518 total variance captured by PC1 and PC2 suggests that other factors may have a stronger influence in this class. 519 520 In contrast, relative water depths (h/D) has a strong negative correlation with scour depths in fine sand (63 to 200 μm) and medium sand (200 to 630 μm). This indicates that as relative water depths increases, scour depths tends 521 522 to decrease in these finer sediment classes. From a physical view, Melling (2015) found out that in similar substrates, seour depths agree well between different geographic locations. Furthermore, Melling (2015) showed 523 524 that turbines located in sandy sediments seemed to show a strong influence of relative water depths on scour, 525 insinuating that geotechnical factors are less influential in granular sediments. The decrease in scour depths with water depth seems unexpected, as in shallow water a greater water depth should lead to a larger boundary layer 526 and thus potentially stronger horseshoe vortex and scour depths (Melville, 2008). However, as explained by Harris 527

and Whitehouse (2014), a weaker down flow and hence a weaker horseshoe vortex can be expected in deeper

water. In deeper water, the hydrostatic component of the total energy at the front of a pile becomes more significant
 compared to the kinetic component, resulting in a more uniform pressure field on the upstream side of the pile and
 a stagnation point closer to the seabed. In addition, the thinner boundary layer implied by shallower relative water
 depths could consequently also lead to greater bed shear stresses, resulting in generally greater sediment mobility.
 The dynamics observed in coarse sand (630 to 2000 μm) and fine gravel (2000 to 6300 μm) are different from the

In these classes, the Reynolds number (Re) and the Froude number (Fr) show significant negative correlations with scour depth, indicating that higher values of these parameters correspond to reduced scour depth. Again, these trends are again somewhat unexpected. In coarser sediments the formation and migration of bed forms is limited, which should results in a stronger correlation with flow parameters and scour depths.

For medium gravel (Figure 5f6300 to 20000 μm), relative water depthdepth has a positive correlation with relative scour depthsdepth, meaning that greater relative water depthsdepth are associated with greater relative scour depthsdepth in coarser sediments. The data points in the cluster can be attributed to the Humber Gateway OWF, which is the only OWF that features clear-water conditions. Given the large grain sizes, a smaller influence of flow parameters on the variability of relative scour depthsdepth should be expected.

544 3.4 Correlation of scour depth with main drivers

534

finer sediments.

Following the PCA (Figure 5), which identified the primary variables influencing <u>relative</u> scour <u>depthsdepth</u> (*S/D*) across <u>sediment classsoil classeses</u>, a Pearson correlation analysis was performed to quantify the strength and direction of these relationships. Figure 6 shows the Pearson correlation results for each cluster and the variable with the strongest correlation, with the red lines representing the linear regression fit and the correlation coefficients shown in red text. The Pearson correlation was calculated by the following equation:

$$R = \frac{\sum (x_i - \bar{x})(y_i - \bar{y})}{\sqrt{\sum (x_i - \bar{x})^2 \sum (y_i - \bar{y})}} \dots (9)$$

551 Taking into account Considering the small number of data points in this sediment cluster, relative scour depths depth 552 at locations with cohesive sediments (Fig. 6a) show a moderate correlation between scour with the mobility 553 <u>parameter.</u> flow intensity $(U_{c,99}/U_{cr})$. For the fine and medium sand clusters, the PCA revealed a similarly strong 554 dependence of relative scour depth on relative water depth-(h/D). Plotting relative scour depthsdepth against relative water depthsdepth now shows a clearer trend and hence dependence for the medium sand sites (Fig. 6c) 555 556 than for the fine sand sites (Fig. 6b). The Pearson coefficients of -0.567 and -0.86 confirm this difference in the 557 dependence of relative scour depth on relative water depth. The correlations of the fine and medium sand clusters 558 are supported by a larger number of data points, increasing the reliability of the findings.

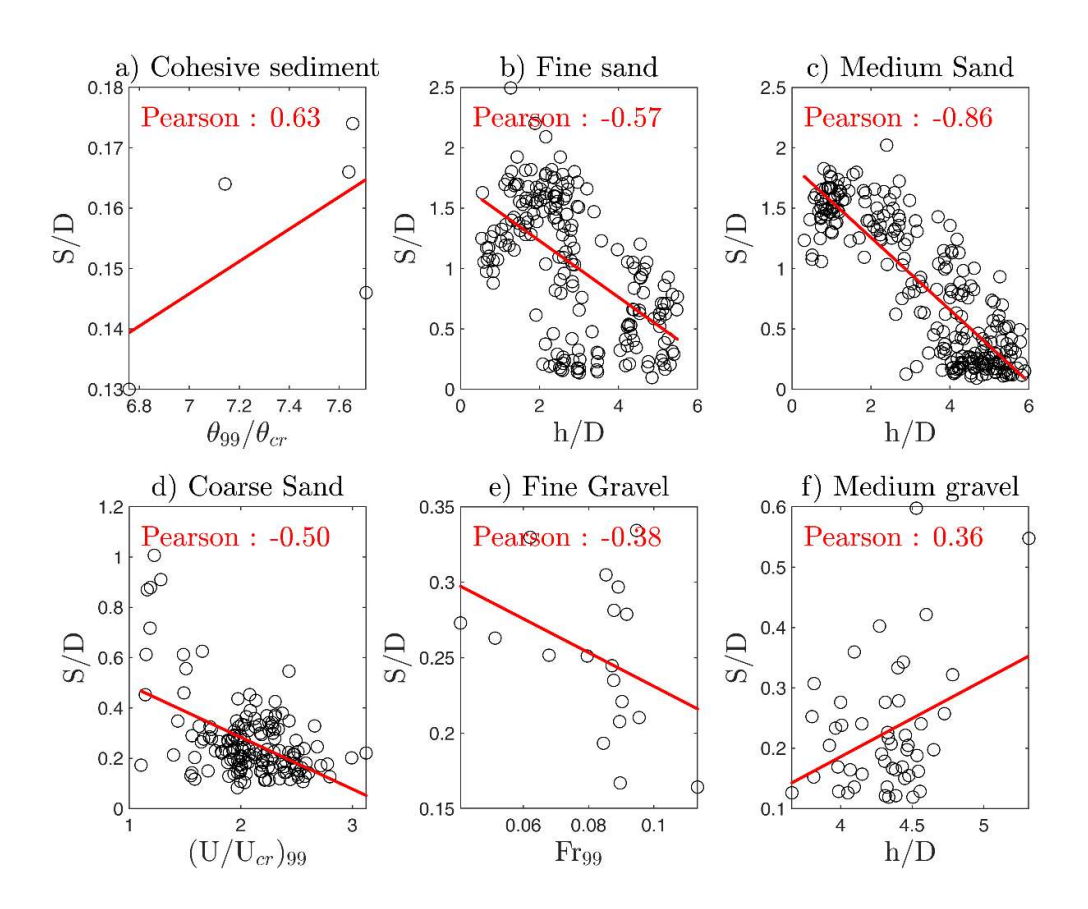


Figure 6: Pearson correlation of representative variables obtained by PCA analysis with relative scour 560 depths depth across different grain sizes soil classes. a) Cohesive sediment $(d_{50} \le 63 \mu m)$ b) 561 Fine sand $(\underline{63} \le d_{50} < \underline{200} \mu m_{63} \text{ to } \underline{200} \mu m)$. c) Medium sand $(\underline{200} \le d_{50} < \underline{630} \mu m_{200} \underline{200} \text{ to } \underline{630} \mu m)$. d) 562 Coarse sand $(\underline{630} \le d_{50} < \underline{2000} \mu m 630 \text{ to } \underline{2000} \mu m)$. e) Fine gravel $(\underline{2000} \le d_{50} < \underline{6300} \mu m 2000 \text{ to } \underline{6300}$ 563 564 μm). f) Medium gravel ($d_{50} \ge 6300 \mu m 6300 \text{ to } 20000 \mu m$). 565 For the coarse sand (630 to 2000 \(\mu\)mFigure 6d), the PCA analysis revealed a negative correlation between relative scour depth and flow intensity. This result directly aligns with the established understanding of live-bed scour 566 behavior in coarse-grained sediments. Once flow intensity surpasses the critical threshold $(U/U_{cr})_{99} \ge 1$, the 567 568 sediment mobilizes, establishing live-bed conditions. In such scenarios, the development of large, well-defined 569 scour holes is consistently observed to be suppressed. This suppression occurs because the continuous transport 570 and replenishment of sediment into the scour region actively works against deep erosion. This dynamic equilibrium 571 of the seabed results in shallower, or inherently more unstable, scour holes when compared to clear-water 572 conditions. In clear-water, where sediment remains immobile, scouring is driven purely by flow-induced vortex 573 action around the structure (Sumer & Fredsøe, 2002; Whitehouse et al., 2011). Consequently, the negative 574 correlation observed in this soil class accurately reflects the inherent limitation of scour growth under the highly 575 mobile conditions characteristic of coarse sandy beds.

the PCA analysis revealed the strongest correlations between seour depth and pile Reynolds number. The 577 578 comparison of these two parameters in Figure 6d confirms the general trend that higher Reynolds numbers lead to lower scour depths, but also shows that scour depths can vary considerably within an OWF despite identical 579 Reynolds numbers. Due to the grid size of the flow data used, the current velocities and hence the pile Reynolds 580 581 numbers vary only slightly within an OWF. For fine gravel (2000 to 6300 µm Figure 6e), the PCA suggests a correlation between relative scour depth and the Froude number, but this is difficult to confirm visually due to the small sample size and narrow Froude 583 584 number range. Since relative scour depth is comparatively small in this class, relationships are less clear, and parameters like Froude number come to the foreground that were not as prominent in finer sediments. A broader 585 distribution of Froude number values would be necessary to confirm this more conclusively. 586 587 analysis showed a very strong correlation between scour depth and Froude number. However, it is difficult to derive this trend between depth and Froude number from the comparison of these two parameters in Figure 6e. 588 Rather, the Froude numbers for the few data points in this group of grain sizes are very close to each other, 589 590 rendering the correlation unreliable. 591 Finally, medium gravel (Figure 6f6300 to 20000 µm) displays a positive correlation between relative scour 592 depthsdepth and relative water depth, with a Pearson coefficient of 0.36. This indicates that larger relative water 593 depths depth correspond to increased scour depths depth, although the range of this increment remains small 594 (between S/D = 0.1 and S/= 0.4-S/D). This variation in scour depth is relatively minor small compared to the trendscorrelations observed in fine and medium sands, where changes in relative water depth yield more 595 pronounced differences in relative scour depths depth. The smaller impact in medium gravel may be attributed to 596 597 the generally greater resistance of larger sediments to scour, even with increasing relative water depths depth. 598 599 to 630 µm Figure 6c), where strong negative correlations between relative scour depthsdepth and relative water 600 depthsdepth are observed. This suggests that significant scour occurs in shallower waters with finer sediments. 601 Such findings highlight the importance of relative water depthsdepth as a key factor influencing scour processes 602 in specific sediment types, emphasizing that scour management and predictions for offshore structures should take 603 sediment characteristics and relative water depthsdepth into account. These results are consistent with the studies 604 from Melling (2015) and Harris and Whitehouse (2014), which also show a decrease in relative scour depthsdepth 605 in finer sediments as relative water depthdepth increases. This negative correlation can be explained by the 606 reduction in bed shear stress with increasing relative water depthdepth, which limits sediment mobilization, 607 particularly in fine and medium sands (Sumer & Fredsøe, 2002; Fredsøe & Sumer, 2014). However, those results 608 are not in agreementdisagree with experimental work where scour around a monopile weakens with reducing 609 relative water depthsdepth (e.g. May and Willoughby, 1990; Whitehouse, 1998). Consequently, relative water 610 depthsdepth is included as a parameter in many empirical formulas, especially in for scour around bridge piles with limited water depth (eg., Laursen, 1963; Hancu, 1971; Breusers et al., 1977; May and Willoughby, 1990; 611 Richardson et al., 2001). Besides that, these insights from field data are critical for the accurate assessment and 612 planning of offshore infrastructure installations, particularly in regions with varying sediment characteristics.

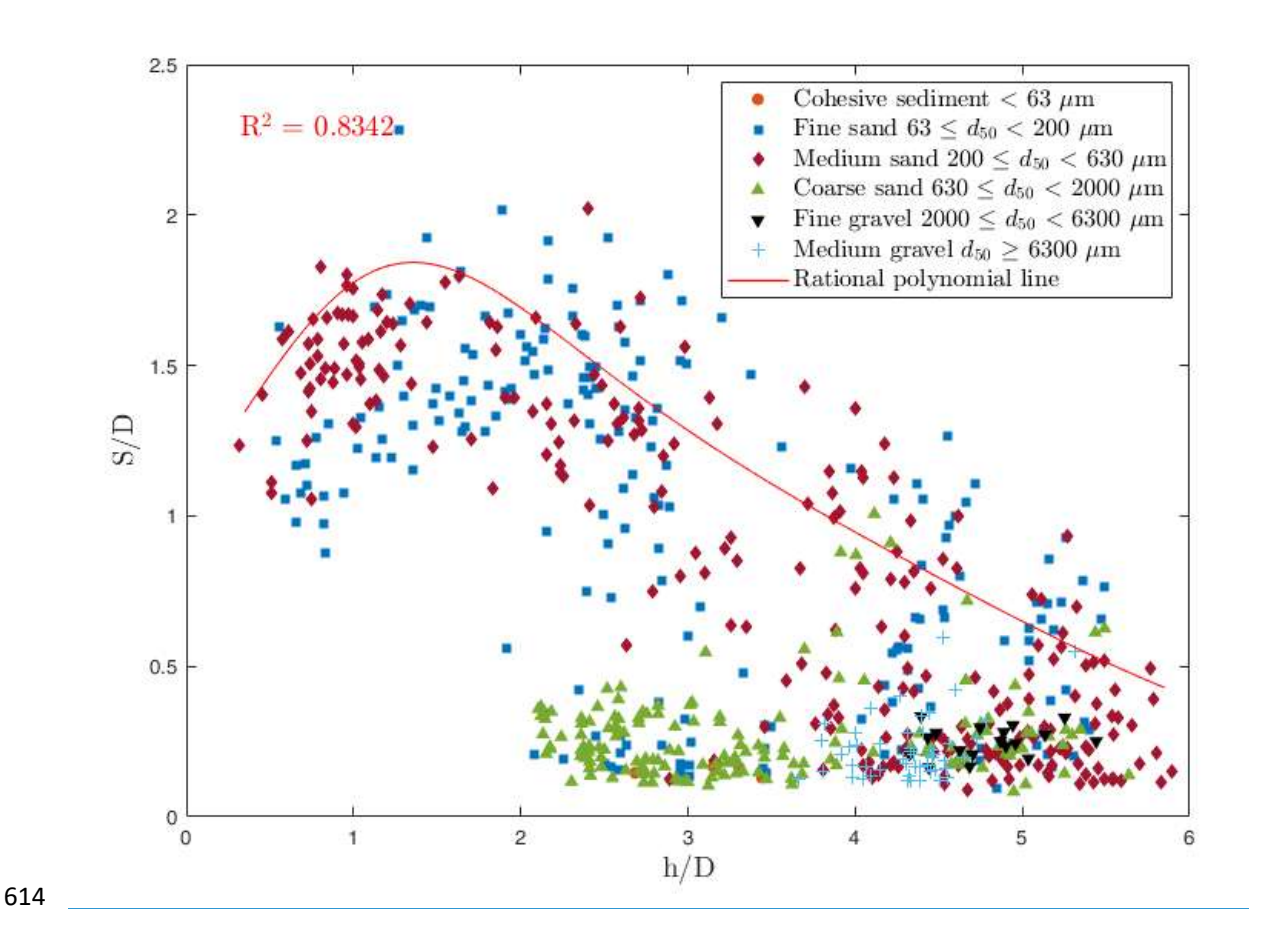


Figure 7: Relative scour depth vs relative water depth, and soil classes. The red rational polynomial line represents a trend based on the course of the 99th percentile. Data points for London Array and Thanet OWFs are included from Melling (2015).

Figure 7 summarizes the findings from the PCA analysis (Figure 4) by plotting the relationship between the relative scour depth and the relative water depth. Relative water depth has shown to be the parameter with the largest correlation influencing relative scour depth. However, it should be noted that relative water depth has a direct effect on other hydrodynamic parameters. For example, not only is the Froude number formed with the water depth, but relative water depth also significantly determines the potential influence of waves on the development of scour, which in this study has also been considered by the Keulegan–Carpenter number. Therefore, it remains unclear whether the influence of relative water depth on relative scour depth is a direct causal factor or an indicator of broader changes in hydrodynamic conditions. Nevertheless, Figure 7 illustrates the comprehensive correlation between the relative scour depth and the relative water depth with the differently colored points representing the studied soils classes.

The trend observed in Figures 6b and 6c is reaffirmed in Figure 7. A distinct relationship exists between the relative scour depth and relative water depth in these two sediment types, i.e. both fine sand $(63 \le d_{50} < 200 \ \mu m)$ and medium sand $(200 \le d_{50} < 630 \ \mu m)$ show that the relative scour depth decreases with increasing relative water depth. This trend appearing throughout the bigger dataset emphasizes a strong negative correlation between relative water depth and relative scour depth for those soil classes. This behavior is consistent with findings from

previous analyses that identified relative water depth as a critical factor in shaping scour dynamics (Whitehouse et al., 2010 and Melling, 2015).

In contrast, for sediments with median grain diameters above coarse sands ($d_{50} \ge 630 \,\mu m$) the relative scour depth remains relatively constant and shows little variability. Figure 7 suggests a generally stable relationship between relative scour depth and relative water depth for these soil classes, where changes in relative water depth do not significantly alter relative scour depth. However, there are a few exceptions. For example, some locations with coarse sand located in deeper water exhibit unexpectedly large relative scour depth. These outliers might stem from site-specific conditions such as dynamic sandbanks and highly variable bathymetry, as seen at the London Array OWF (Sturt et al., 2009). These unique environments, characterized by flow recirculation and sediment mobility, can lead to deviations from expected scour behavior (Melling, 2015). The results for fine and medium sands suggest a potential influence of relative water depth in reducing relative scour depth. Although these results are preliminary, they provide a first step in understanding how offshore wind OWES could affect sediment redistribution in regions dominated by these sediment types and small relative water depth

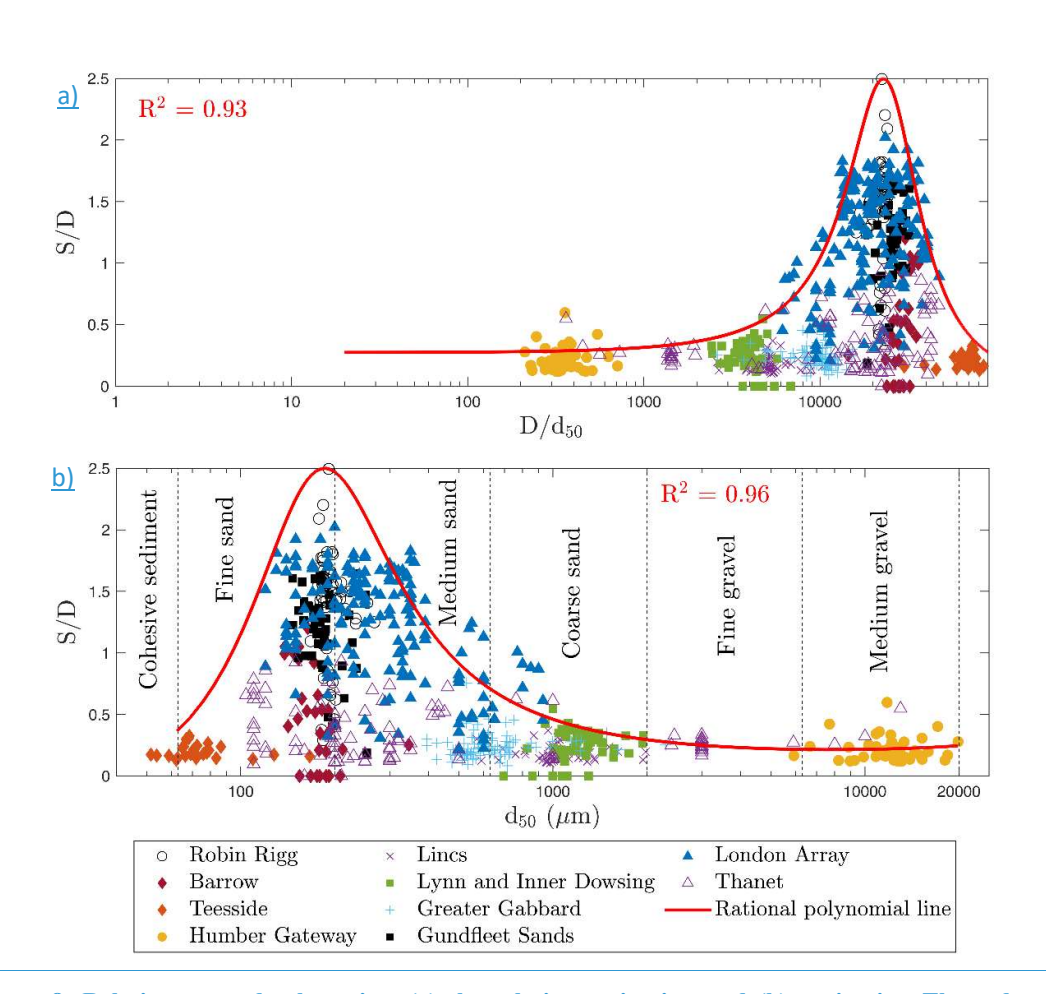


Figure 8: Relative scour depth against (a) the relative grain size, and (b) grain size. The red rational polynomial line gives the approximate upper limit of S/D, based on the course of the 99th percentile, for various d_{50} . Data points for London Array and Thanet OWFs are included from Melling (2015).

Figure 8a summarizes the findings from the PCA analysis (Figure 4) by plotting the relationship between the relative scour depth and relative grain size across all the sampled locations. Figure 8b is also shown here to support

figure 8a by representing the data in terms of the grain size, allowing the comparison of dimensional and non-653 654 dimensional relative grain size. Figure 8a, reveals no clear trend between relative scour depth and relative grain 655 size, indicating that the dimensionless grain size ratio alone does not adequately capture the relationship between sediment properties and scour depth in field data. Sheppard et al. (2004) observed a clear trend of S/D decreasing 656 $\frac{\text{for }D}{d_{50}} > 50$ in laboratory experiments, which is not consistent with our results. However, field data show 657 much weaker dependence due to natural variability in sediment structure and hydrodynamic forcing 658 659 On the other hand, Figure 8b illustrates a discernible trend where the largest relative scour depth occurs predominantly in fine to medium sands (R²= 0.8407), as indicated by the rational polynomial line which 660 approximates the upper limit of relative scour depth for various grain size. The trend shown in Fig. 8b is well 661 662 explained. In general, the mobility potential of the sediments decreases with increasing grain size, which leads to lower relative scour depth for coarser sediments. Very fine sediments, on the other hand, are subject to the 663 664 influence of cohesion forces that reduce their erodibility, which also leads to lower relative scour depth. Therefore, 665 fine and medium sandy sediments have the largest scour potential, which is reflected in the data of Fig. 8b. The 666 different symbols represent the OWF, highlighting the geographic spread and variability within the dataset. 667 However, it is important to note that most of the data points fall within the range of fine to medium sands, 668 potentially skewing the interpretation. 669 670 671 672 673 674

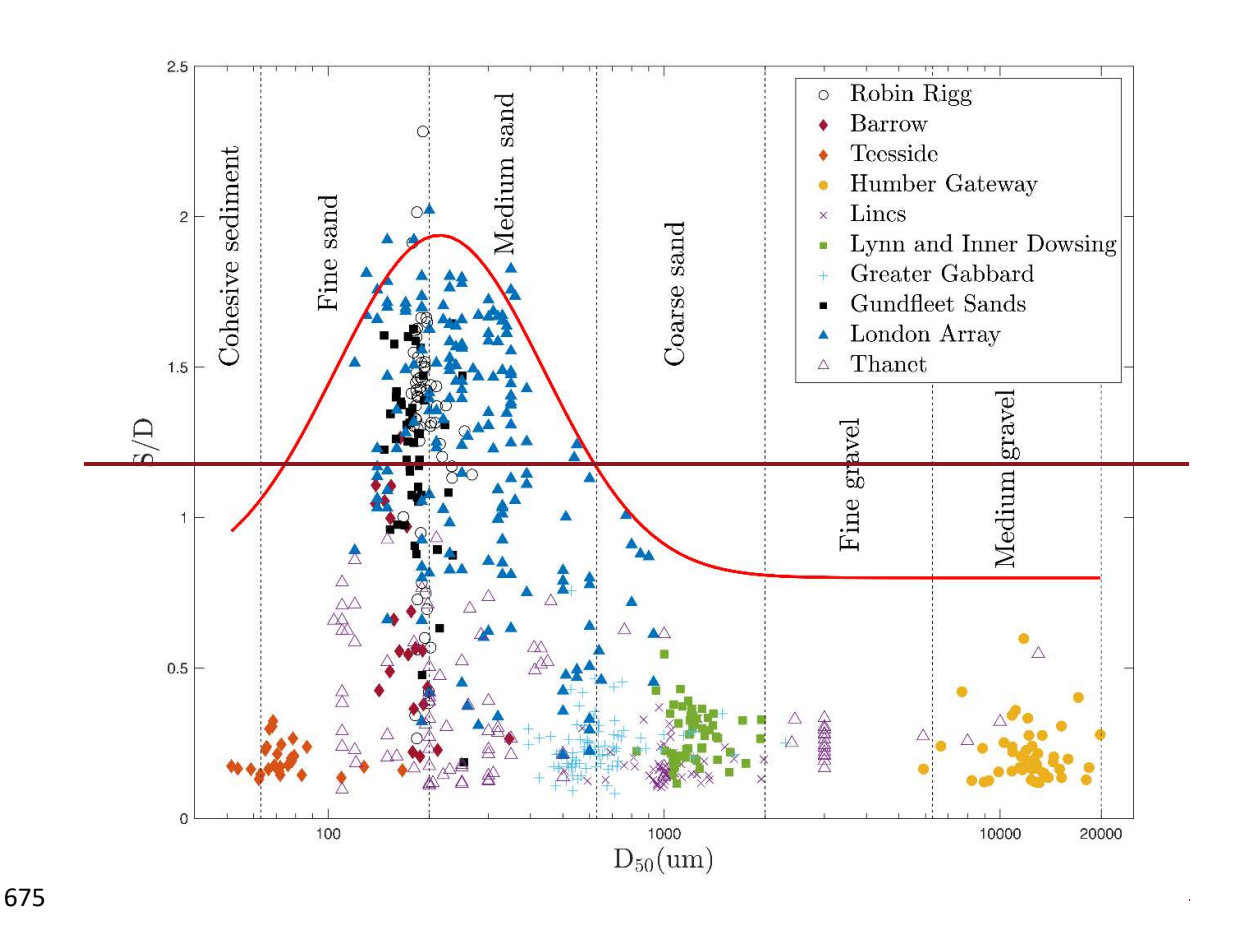


Figure 7: Relative scour depths S/D against grain size D₅₀. Red line gives approximate upper limit of S/D for various D₅₀. Data points for London Array and Thanet OWFs are included from Melling (2015).

Figure 7 summarizes the findings from the PCA analysis (Figure 4) by plotting the relationship between the relative scour depth (S/D) and grain size D_{S0} across all the sampled locations. This figure illustrates a discernible trend where the largest scour depths scour occur predominantly in fine to medium sands, as indicated by the Gaussian fit line which approximates the upper limit of S/D for various D_{S0} . This visualization captures the broad distribution of data points and highlights the significant influence of grain size on scour depths, confirming the results PCA of the PCA that identified Dd_{S0} as a key factor in scour dynamics. The trend shown in Fig. 7 is well explained. In general, the mobility potential of the sediments decreases with increasing grain size, which leads to lower scour depths for coarser sediments. Very fine sediments, on the other hand, are subject to the influence of cohesion forces that reduce their crodibility, which also leads to lower scour depths. Therefore, fine and medium sandy sediments have the largest scour potential, which is reflected in the data of Fig. 7. The different symbols represent the OWF, highlighting the geographic spread and variability within the dataset. However, it is important to note that the majority of the data points fall within the range of fine to medium sands, potentially skewing the interpretation.

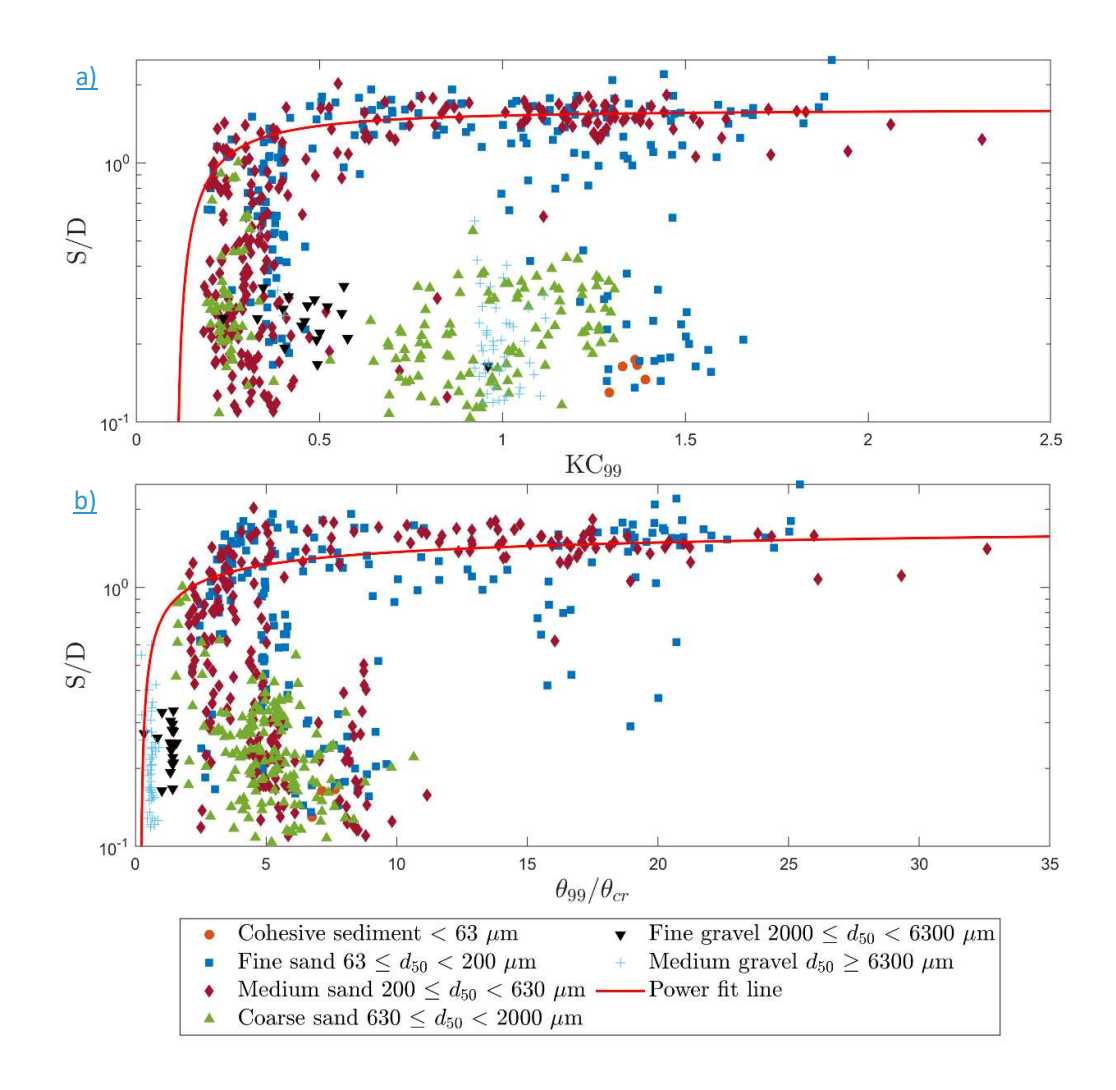


Figure 9: Relative scour depth against the a) Keulegan-Carpenter number and b) the mobility parameter. Red line gives the power fit line based on the 99th percentile of the data of relative scour depth for various d_{50} . Data points for London Array and Thanet OWFs are included from Melling (2015).

The third and fourth parameters, that correlate with the relative scour depth, are the Keulegan-Carpenter number and the mobility parameter as identified by the PCA. Figure 9a shows the correlation between the relative scour depth and the Keulegan-Carpenter number, revealing a distinct increase of relative scour depth with increasing Keulegan-Carpenter number up to $KC_{99} = 0.5$. Above this value, relative scour depth shows little variation with further increase of the Keulegan-Carpenter number, which reaches a maximum value of 2.5 in this field dataset. Those results are generally consistent with findings from previous studies (e.g., Qu et al., 2024; Sumer & Fredsøe, 2002), which indicate that scour development is strongly dependent on KC_{99} at lower values, but becomes less sensitive as KC_{99} increases. However, experimental studies often focus on wave regimes with KC numbers greater than 6, since it has been established that this is the threshold for generating a horseshoe vortex. Despite considering the 99th percentile of KC numbers over the time period in question, the KC numbers are much smaller for the field conditions presented herein. This strengthens the argument for further scour research to focus on boundary conditions with low KC values.

708 Figure 9b shows the correlation between relative scour depth and mobility parameter, comparing the Shields parameter with its critical threshold for sediment motion, and revealing a distinct increase of relative scour depth 709 710 with increasing mobility parameter up to approximately $\theta_{99}/\theta_{cr}=5$. At higher mobility values (typically above 5– 10), the increase in scour depth tends to stabilize. This trend aligns with experimental observations from Sumer et 712 al. (2013), Chiew (1984), and others, which describe similar stabilization of scour depth under fully mobile 713 conditions. Notably, the response also varies with sediment type: coarser sediments exhibit low relative scour 714 depth values even at high mobility ratios, likely due to their higher resistance to entrainment and potential armoring 715 effects. In contrast, finer sediments (e.g., d_{50} < 200 μm) show a steeper increase in scour depth, reflecting their greater susceptibility to hydrodynamic conditions. 716

Overall, Figure 9a and 9b emphasize the nonlinear and sediment-dependent nature of scour formation. The separation of trends by soil class supports the need for sediment-specific scour prediction models, as also suggested in previous studies (e.g., Whitehouse et al., 2011; Sumer & Fredsøe, 2002). The results provide empirical evidence of this dependency using field-scale data, bridging a critical gap between controlled experiments and real-world conditions.

722

723 .

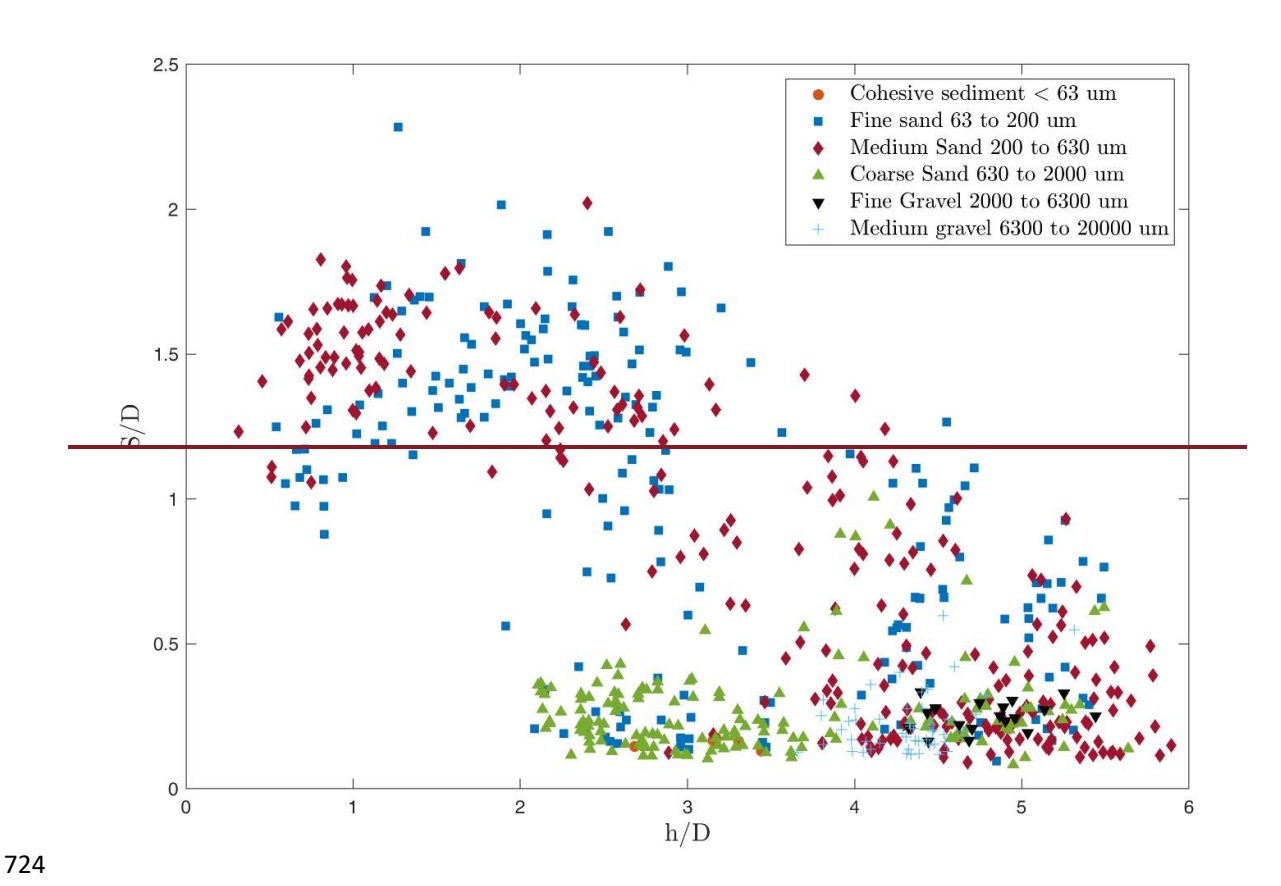


Figure 8: Relative scour depths vs relative water depths, and sediment classification. Data points for London
Array and Thanet OWFs are included from Melling (2015).

In addition to the influence of sediment grain size, relative water depth has been shown to be the most important 727 728 factor influencing relative scour depth. However, it should be noted that water depth has a direct effect on other 729 parameters. For example, not only is the Froude number formed with water depth, but water depth also significantly determines the potential influence of waves on the development of scour, which in this study has so 730 731 far only been considered via the significant wave height. It is therefore not clear whether the influence of water 732 depth on scour depth is a causal factor, or whether the cause of changes in scour depth is related to changes in flow 733 conditions caused by changes in water depth. Nevertheless, Figure 8 illustrates the comprehensive correlation 734 between the relative scour depth (S/D) and the relative water depth (h/D), with the differently colored points 735 representing the studied sediment clusters.

736 The trend observed figures 6b and 6c is reaffirmed in Figure 8. A distinct relationship exists between the scour 737 depth and water depth in these two sediment types, i.e. both fine sand (63 to 200 μ m) and medium sand (200 to 738 630 μ m) show that the scour depth decreases with increasing water depth. This trend appearing throughout the 739 bigger dataset emphasizes strong negative correlation between water depth and scour depth for those sediment 740 classes. This behavior is consistent with findings from previous analyses that identified water depth as a critical 741 factor in shaping scour dynamics (Whitehouse et al., 2010 and Melling, 2015).

742 In contrast, for sediments with median grain diameters above coarse sands $(D_{ED} \ge 630 \, \mu m)$ the scour depth remains 743 relatively constant and shows little variability. Figure 8 suggests a generally stable relationship between scour 744 depth and water depth for these sediment classes, where changes in water depth do not significantly alter scour depth. However, there are a few exceptions. For example, some locations with coarse sand located in deeper water 745 746 exhibit unexpectedly large scour depths. These outliers might stem from site-specific conditions such as dynamic sandbanks and highly variable, as seen at the London Array OWF (Sturt et al., 2009). These unique environments, 747 characterized by flow recirculation and sediment mobility, can lead to deviations from expected scour behavior 748 749 (Melling, 2015). The results for fine and medium sands suggest a potential influence of water depth in reducing scour depth, which could have implications for sediment transport and the marine environment. Although these 750 751 results are preliminary, they provide a first step in understanding how offshore wind turbines could affect sediment 752 redistribution in regions dominated by these sediment types and small water depth.

753 754

3.5 Detailed analysis of scour patterns for selected OWFs

Following the observed overall trend shown in Figure \$7, this section moves on to examine scour patterns within individual OWFs, such as Robin Rigg, Lynn and Inner Dowsing, and London Array. This specific analysis will assess whether the global relationship between relative scour depthsdepth, dD_{50} , and relative water depthsdepth holds under the unique environmental conditions of each site. This section aims to further our understanding of the dynamics between sediment characteristics and scour processes by a detailed analysis of the variation within each wind farm to determine if these global correlations are consistent at the local scale or if there are deviations due to site-specific factors.

_

3.5.1 Robin Rigg OWF
 Robin Rigg is presented and discussed in this section as this OWF has the largest overall relative scour depthsdepth
 of all the OWFs. This detailed analysis will help to investigate whether the negative correlation between relative
 scour depth-S/D and relative water depth-h/D observed globally in Figure 78 holds true under variable
 geotechnical conditions, taking into account that sediment grain sizes range from fine to medium sands.

767 Figure 910 shows the distribution of relative scour depthsdepth at Robin Rigg in relation to the variable 768 geotechnical and hydrodynamic site conditions. This sequence begins with Figure 9A, showing the spatial 769 distribution of scours measured one year after turbine installation. A significant variation in relative scour depthsdepth in different areas of the OWF can be observed, with the deeper relative scour depthsdepth mainly 771 located in the northeastern part, particularly around turbines OWES D7, C6, B5 and B4, which are located in the 772 shallowest waters. Figure $\underline{109}$ B shows the spatial distribution of the median grain diameter $\underline{P}d_{50}$ in the uppermost 773 sediment layer in 2005, with sediment sizes predominantly in the range of fine to middle sand (182 µm to 268 774 μm). Turbines OWES in areas with finer sands, such as D4, D5, and D6, are observed to generally experience the 775 large scour, consistent with previous observations by Whitehouse (2006) that finer sand substrates are more 776 susceptible to scour.

Figure 109C shows the correlation of relative scour depth S/D and relative water depth h/D, classified by colored points which represent sediment grain size from figure 9B. Contrary to the clear negative correlation between relative scour depth S/D and relative water depth h/D observed globally in Figure 8, Figure 910C shows a wide distribution of data points with no clear trend, suggesting that local factors in addition to relative water depths and sediment type have an influence on scour at this site.

For additional insight, Figures 109D and 109E show the distribution of the directions of significant wave heights, as well as the directions of current velocity magnitudes one-year period, prior the post scan. The highest wave heights came predominantly from the southwest, which should influence sediment mobility and thus scour structures along this direction and especially in shallow relative water depthsdepth where wave-induced shear stresses should be higher. Similarly, the tidal current, with its main directions of south-west and north-east, should result in a change in relative scour depthsdepth along this main axis. However, a clear trend of relative scour depth changing in this direction is not given for Robin Rigg.

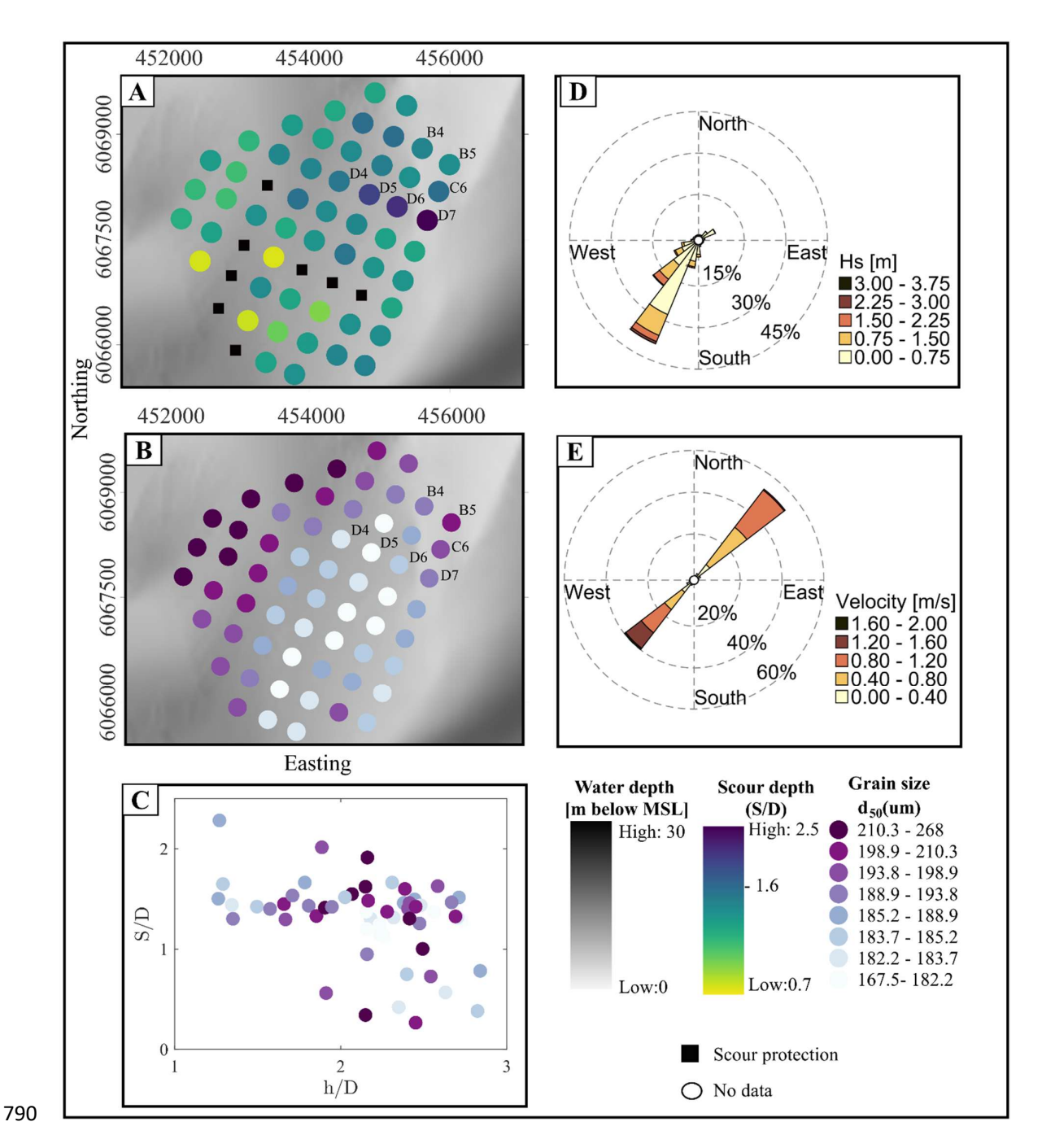


Figure 910: A) Spatial distribution of relative scour depthsdepth (S/D) from 2008-2009 at Robin Rigg OWF.

B) Grain-size distribution. C) Relative scour depthsdepth vs relative water depthsdepth, and grain size classification D) Significant wave heights E) Current velocities.

This comprehensive analysis using Figures 109A to 910E shows that while trendscorrelations obtained from global findings provide a useful baseline for understanding scour, the actual scour observed at Robin Rigg does not necessarily follow those trendscorrelations. While the distribution of relative scour depthsdepth appears to be strongly influenced by local environmental conditions such as sediment type, waves and currents, the dominant influence among these cannot be clearly identified, rather the distribution of relative scour depthsdepth appears to be due to the interaction of all influences.

The discrepancies between the local scour behavior at Robin Rigg and the broader trendscorrelations observed in Figure 8 underscore the need for site-specific assessments. Such detailed analyses are critical to the development of effective scour management and mitigation strategies tailored to the unique conditions of each offshore wind farm.

804 3.5.2 Lynn and Inner Dowsing OWF

Lynn and Inner Dowsing was chosen as a further example as this OWF had the lowest relative scour depthsdepth 805 806 of all the OWFs investigated and is also characterized by coarse to very coarse sands. Figure 101 provides the 807 same analysis as Figure 910 by providing insight into how local conditions compare to the global trend seen in 808 Figure 78. Figure 10A shows the spatial distribution of relative scour depthsdepth (S/D) measured from 2007 to 2010. Figure 101A shows that the largest relative scour depthsdepth are mainly concentrated in the Inner Dowsing 809 area, especially around turbines OWES ID1, ID2, ID8, ID9, ID12, ID24, and ID30. Except for turbine L21, which 811 has the deepest relative scour depthsdepth in the entire wind farm and which is located at the southeastern end. 812 The significant relative scour depthsdepth observed at certain locations (e.g., D30, L21) are related to cable exposure (EGS Ltd, 2012; EGS Ltd, 2013), while smaller relative_scour depthsdepth are more common in the 813 814 southern region. Overall, the spatial distribution shows a slight trend of increasing relative scour depthsdepth from 815 south to north.

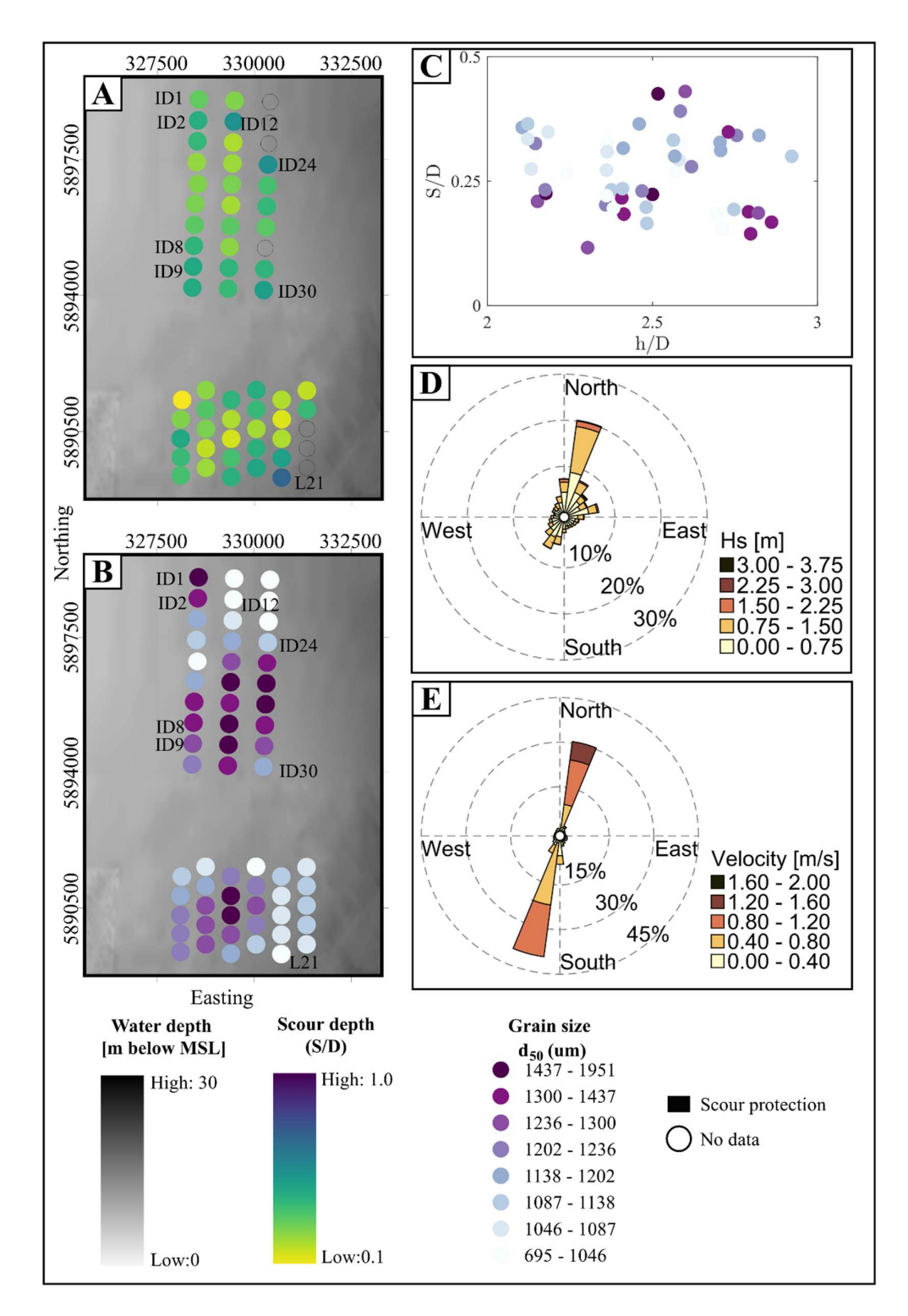


Figure 101: A) Spatial distribution of relative scour depthsdepth-(S/D) at Lynn and Inner Dowsing OWF from 2007-2010. B) Grain-size distribution. C) Relative scour depthsdepth vs relative water depthsdepth, and grain size classification. D) Significant wave heights E) Current velocities.

820 Continuing with the spatial overview, Figure 101B introduces the spatial distribution of dD_{50} median grain sizes, 821 which shows a range from coarse to very coarse sands (695 to 1951 μm).. The correlation between relative scour

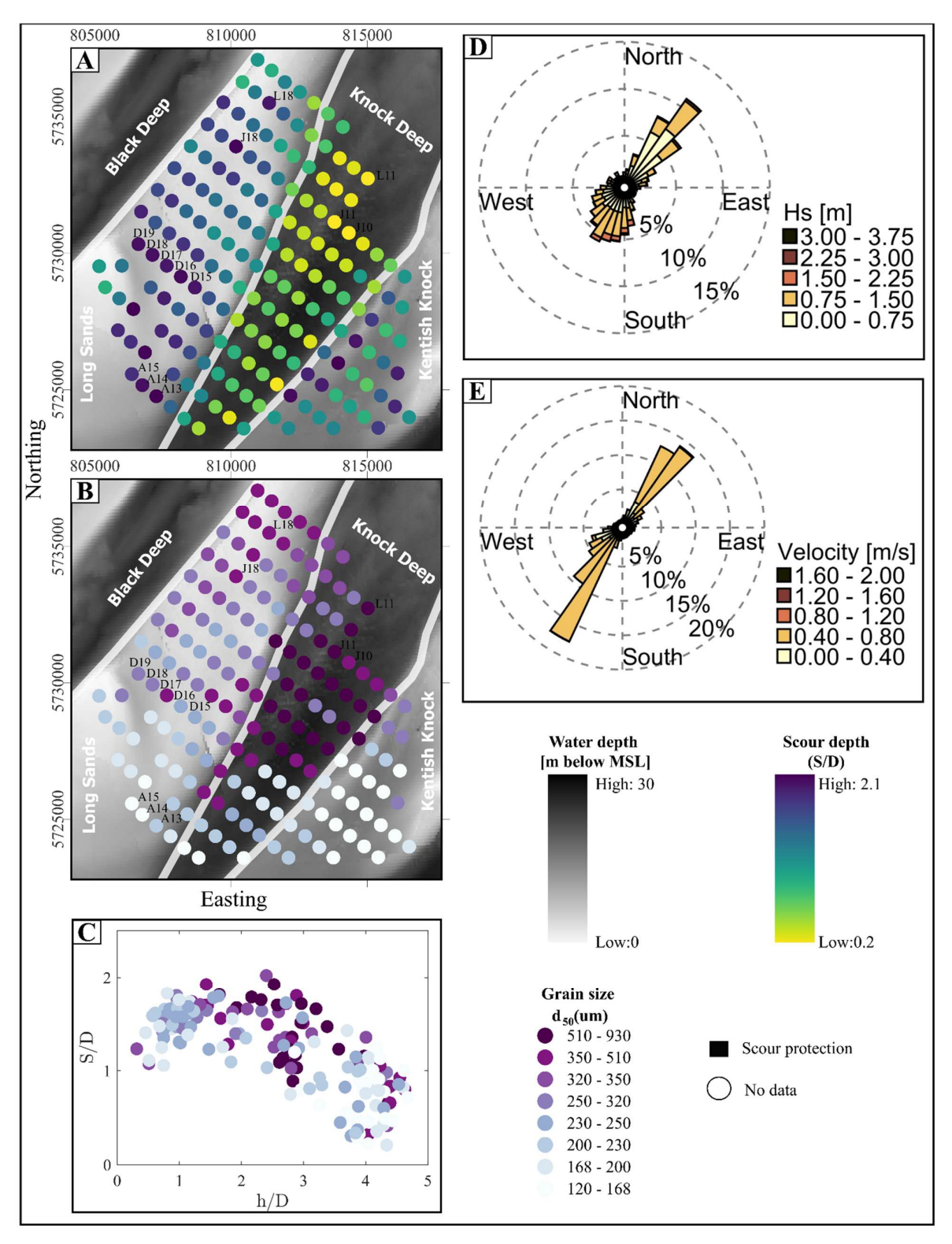
depth (S/D)-and relative water depth (h/D) is examined in Figure 101C.- Similar to Robin Rigg, this OWF does not display the negative correlation as seen globally in Figure 8, suggesting that additional local factors may

824 significantly influence <u>relative</u> scour <u>depths</u>depth.

Consequently, the significant wave heights and current velocities from hindcast data are shown in Figure 10D and 10E. The highest wave heights, observed from the northeast, and strong tidal currents flowing from southwest to northeast, highlight the dynamic environmental forces at play. The presence of the largest <u>relative</u> scour depthsdepth in the Inner Dowsing area align with the direction of the highest tidal current velocities (Fig. 101E) recorded in the northeast part as well the main direction of waves. Therefore, the direction of both tidal current and waves likely play a significant role for the scour development in this wind farms, as the seabed conditions and relative water depth locally do not exhibit a distinct correlation.

832 3.5.3 London Array OWF

Following the previous results, the analysis for London Array OWF shows a wide range of relative scour depthsdepth from 0.2 S/D = 0.2 to 2.1 S/D = 2.1. This variability differs markedly from the consistently larger 834 relative scour depthsdepth observed at Robin Rigg and the limited maximum depthsdepth of up to $\frac{1.0 \text{ S}}{D} = 1.0$ 835 836 at Lynn and Inner Dowsing. "The area of London Array OWF is characterized by an alternating pattern of deep 837 channels (Black Deep, Knock Deep) and sandbanks (Long Sands, Kentish Knock). These topographic features significantly contribute to the local scour patterns. Water depths depth at this site range from 0 to 30 m, with Long 838 839 Sands known for its significant variations in bed elevation but general stability of position. Meanwhile, Knock 840 Deep is notable for its eastward shift over time, which has widened the channel and maintained a constant bed 841 level.



843 Figure 11 Figure 12: A) Spatial distribution of relative scour depthsdepth-(S/D) at London Array OWF from 2010-2014. B) Grain-size distribution. C) Relative scour depthsdepth vs relative water depthsdepth, and Grain size classification. D) Significant wave heights and E) Current velocities. Relative scour depth data S/D and grain size D₅₀₀ data are used from Melling (2015)

844 845

In Figure 124A, the distribution of relative scour depthsdepth shows that the variation in scour is strongly influenced by the underlying topography, with significantly greater relative scour depthsdepth on the sand banks compared to the channel. Additionally a trend of increasing relative scour depths depth is observed from northeast to southwest, which is particularly notable in the channel area. The smallest scour is observed in the northern part of Knock Deep with a ratio of 0.2 S/D = 0.2 and the largest in the southern part of Long Sands with 2.1 S/D = 0.22.1. The differences in relative scour depths depth can be derived directly from the seabed topography, with greatest average relative scour depthsdepth found in the Long Sands with $\frac{1.53}{5}$ S/D = 1.53, followed by Kentish Knock (S/D = 1.37), and then Knock Deep (S/D = 0.77) with the smallest average. The sediment distribution across this OWF, shown in Figure 11Figures 12B, ranges from very fine to coarse sands. Coarse sands can be found in Knock Deep, where generally the smallest relative scour depthsdepth are seen (e.g., L11, J10 and J11). Furthermore, the largest relative scour depthsdepth are noticed in the southern part of Long Sands (e.g. A13-A15, D15-D19, J18 and L18), where the sediment varies from very fine to fine medium sands. There is therefore a reasonable correlation between grain size and relative scour depth, which is consistent with the previously observed global trend. Additionally, Figure 11Figures 12C shows a negative correlation between relative scour depth S/D and relative water depth h/D aligning with the global trend observed in Figure 8, i.e. that shallower relative water depths depth can be associated with deeper scour, while deeper waters tend to have reduced relative scour depthsdepth. This trend may be explained by the findings of Hjort (1975), who demonstrated that bed shear stress decreases with increasing relative water depth for the same flow and structure diameter, potentially leading to reduced scour at greater depthsdepth. However, as the relative water depth in the London Array OWF changes simultaneously with the sediments, i.e. coarser grained sediments are present in the deeper water depthsdepth of Knock Deep, the cause of the different relative scour depthsdepth cannot be clearly attributed to either the sediments or the water depth. Other hydrodynamic, environmental, and topographic factors also play a critical role in shaping these patterns at this OWF, underscoring the complexity of the influences involved.

Significant wave heights and current velocities, as shown in Ffigures 124D and 124E, provide important insights into the scour dynamics at the London Array. These figures show that, in addition to relative water depthsdepth and sediment grain sizes, wave and current dynamics might be critical factors at this wind farm. The predominant direction of both waves and currents is northeast to southwest, consistent with the estuarine influence of the area, where river discharge also significantly affects hydrodynamic conditions. This influence is particularly evident at the Long Sands and Kentish Knock sandbanks, which are shaped by the combined action of waves and currents (London Array Ltd, 2005).

 Figure 11Figures 12D shows that the highest wave heights are observed coming from the northeast, with values exceeding 3.0 m, and lower wave heights propagating from the southwest. This gradient in wave height suggests a correlation with increased relative scour depthsdepth in regions exposed to higher wave energy, suggesting a strong link between wave dynamics and seabed modification. However, estimated KC₉₉ numbers remained relatively low across most sites, indicating limited wave-induced orbital motion near the seabed. This suggests that wave action plays a secondary role in scour development compared to currents. Similarly, Figure 11Figure 12E highlights a larger number of strong currents coming from the southeast. These higher velocities correspond to areas with more pronounced relative scour depthsdepth, highlighting the role of strong currents in influencing sediment transport and depositional patterns.

In addition, the local tidal dynamics vary significantly across the wind farm, with the flood tide dominating the southern banks and the ebb tide more influential on the northern banks (Kenyon and Cooper, 2005). This variation is due to the sheltering effect of the sandbanks, which are slightly offset from the orientation of the ebb tide, and is particularly pronounced at Long Sands (London Array Ltd, 2005). The interplay of river discharge, wind stress,

892 tidal surge and density driven currents follow the pathways created by the existing topography, further

893 complicating the hydrodynamic environment and its effect on scour at the London Array OWF.

894 After analyzing the <u>relative</u> scour <u>depthsdepth</u> at 9 wind farms and with different ranges of <u>relative</u> scour

895 depthsdepth, the variation of relative scour depthsdepth can also be noticed in individual OWFs, as in the case for

896 London Array OWF.

897 4. Discussion

4.1 Discussion of Limplications for scour predictions for OWFs 898 899 Overall, this study extends the investigation of scour dynamics to a regional scale by analyzing correlations between relative scour depth and site conditions across multiple OWFs to identify consistent scour patterns and 901 trendscorrelations. The PCA analysis highlights a significant negative correlation between larger relative scour 902 depthsdepth(S/D) with relative water depth(h/D), and finer sediment types (particularly fine and medium sands), suggesting that relative water depth plays a critical role in scour processes, confirming the correlations observed 903 with previous Whitehouse et al. (2010) and Melling (2015) for field data. The decrease of the relative scour depth 904 905 with decreasing relative water depth seems unexpected and contradicts common scour prediction approaches such 906 as. Breusers et al. (1977), which however are often derived for flow conditions with shallow relative water depth. 907 Harris and Whitehouse (2014) argued that in deeper water, a weaker downflow and hence a weaker horseshoe 908 vortex can be expected, ultimately leading to smaller scour depth. This finding implies that scour prediction 909 approaches should place greater emphasis on relative water depth, particularly in offshore environments where 910 deeper flow conditions dominate. A second notable correlation was identified between the relative scour depth with the relative grain size. 1, -a 911 finding consistent with sediment transport theories that suggest finer noncohesive grains are more susceptible to 912 913 mobilization by hydrodynamic forces. TTthis broad correlation, observed consistent across different geographic

914 locations and environmental conditions, reinforces the universality fundamental role of sediment size as a

915 fundamental factor in scour processes, as documented in the extensive work of Vanhellemont et al. (2014) and

916 Rivier et al. (2016). Given the large underlying database, this study adds weight to the argument for the universal

917 incorporation of detailed sediment characteristics into scour assessment practices.

However, the analysis also showed indicates that the sediment erodibility the strong influence of the erosion potential of the sediments in the field alone cannot fully account for the describe all observed variability in relative scour depth ations. The PCA analysis also provided further reveals a a strong negative positive correlation between the relative scour depth and both the Keulegan Carpenter number and the sediment mobility parameter. The strong positive correlation with KC₉₉ supports previous studies (Sumer and Fredsoe, 2001; Qu, 2024), highlighting the

923 importance of flow unsteadiness that is typical in tidal and wave-dominated environments. Similarly, the positive

924 association with the mobility parameter underscores its relevance as a key indicator of sediment entrainment and

925 a useful metric for distinguishing between different sediment transport regimes.

926 observed between relative scour depth() and relative water depth (), particularly in fine and medium sand 927 sediments, suggesting that the relative water depth () plays a critical role in scour processes, confirming the

trendscorrelations observed by Whitehouse et al. (2010) and Melling (2015) for field data. The decrease of the 928 929 scour depth with decreasing water depth seems unexpected and contradicts common scour prediction approaches like e.g. Breusers et al. (1977), which however are often derived for flow conditions with shallow water depth. 930 Harris and Whitehouse (2014) argued that in deeper water, a weaker downflow and hence a weaker horseshoe 931 932 vortex can be expected, ultimately leading to smaller scour depth. As the depth increases, the hydrostatic 933 component of the total energy at the front of the pile increases relative to the kinetic component. Additionally, the reduction in boundary layer thickness, induced by decreased water depths, has the potential to enhance bed shear 934 935 stresses, thereby increasing sediment mobility. For certain sediment groups, the PCA demonstrated a stronger 936 eorrelation with the pile Reynolds number or the Froude number. Thisese findings underscores a complex dynamic 937 that is frequently oversimplified in existing models. The results indicate a necessity to incorporate nonlinear hydrodynamic models into scour prediction frameworks. The results of the PCA reveal the necessity for a 938 939 diversified approach to the modeling of scour in complex field conditions, which extends beyond the scope of 940 traditional uniform applications.

941 This analysis demonstrates that individual OWFs exhibit unique environmental and sediment conditions, which 942 can either amplify or moderate broader trendscorrelations. The London Array OWFs serves as a prime example of the predictive reliability of observed regional trendscorrelations, as local data closely mirrors general 943 944 trendscorrelations. Conversely, sites such as Robin Rigg and Lynn and Inner Dowsing exhibit deviations from 945 these trendscorrelations due to their distinct sediment compositions and hydrodynamic conditions, underscoring 946 the necessity for site-specific adjustments to scour prediction models. These findings underscore the intricacy of 947 employing global models on a local scale and underscore the significance of site-specific data in validating and 948 refining these models to enhance their accuracy and applicability.

949 5-4.2 Discussion of Llimitations and future research

Although this study provides a detailed analysis of <u>relative</u> scour <u>depthsdepth</u> at nine OWFs, certain limitations must be addressed to improve the interpretation of the findings. Although the dataset spans multiple years, it represents snapshots in time and may not fully capture the dynamic evolution of scour processes under fluctuating metocean conditions (Matutano et al., 2013; Carpenter et al., 2016). Hindcast data, while valuable for long-term trendscorrelations, are often based on limited spatial resolution that may underestimate short-term extreme events such as storm surges or localized current variations (Whitehouse et al., 2010; Sturt et al., 2009).

Using PCA is effective in identifying dominant linear relationships between relative scour depthsdepth and key 956 957 variables; however, it may miss critical nonlinear interactions that drive scour processes (Schendel et al., 2020; 958 Lyu et al., 2021). While this study incorporates, Pparameters such as the Keulegan-Carpenter - KG-number and 959 Shields parameter the mobility parameter, the accuracy of these parameters are limited by temporal resolution and 960 data availability. which account for sediment motion initiation and hydrodynamic forces, could not be reliably 961 determined in this study due to data limitations. Given their importance in understanding sediment transport and 962 scour development Valuable insight was provided into the role of hydrodynamic forcing on sediment mobility 963 through their inclusion; however, more detailed and site-specific input data are needed so that their predictive 964 potential can be fully exploited (Sheppard et al., 2004; Zhao et al., 2012), future studies should prioritize the 965 inclusion of these dimensionless parameters to provide a more robust assessment and comparison of scour 966 processes.

The next step in this research is to develop data-driven models and investigate the broader implications for regional sediment dynamics. Future studies will focus on OWFs located in fine and medium sands where significant scour

970 understand the mechanisms that drive scour, particularly in areas that are susceptible to substantial sediment 971 mobilization. 972 Finally, while the present study focused on localized scour processes, the cumulative effects of OWF structures 973 on regional sediment transport and marine ecosystems remain a significant knowledge gap (Christiansen et al., 974 2022; Schultze et al., 2021). Future research must employ interdisciplinary methodologies to rigorously assess the ecological impacts of sediment mobility and scour on marine habitats. By integrating regional sediment transport 975 976 models with comprehensive ecological assessments, we can optimize offshore wind energy development to meet 977 both sustainability and environmental protection goals, ensuring long-term benefits for infrastructure resilience

activity is observed. By focusing on these environments, we aim to improve prediction capabilities and better

979 56 Conclusion

and marine ecosystem health.

969

978

980

983

984

985

986

987

988

989

990

991

992

Achieving the European Union's (EU) offshore wind energy targets requires development of OWFs in regions 981 with diverse and often poorly understood meteoceanic and geophysical conditions. However, this demand 982 underscores critical knowledge gaps regarding the interaction of these installations with the marine environment, particularly with respect to scour processes and sediment mobilization. A comprehensive understanding of scour dynamics is essential, not only to ensure structural integrity, but also to assess potential impacts on regional sediment transport and broader ecosystem functions.

In this study, high-resolution bathymetry data were used to analyze field-measured relative scour depths depth of 460 monopiles across nine British OWFs. The analysis included a PCA in which eight hydrodynamic and geotechnical variables were considered to identify the dominant driver influencing relative scour depths depth variability. This analysis provided a basis for understanding the primary correlations between relative scour depthsdepth and metocean site conditions, but also highlighted the complexity of these relationships, requiring further refinement.

The main conclusions can be summarized as follows:

993 994

995

996

997

998

999

1000

1001

1002

1003

1004

1005

1006 1007

1008

(1) Universal -drivers of scour: Across all nine OWFs, the PCA identified D₅₀, as one of the main drivers in influencing scour depthsdepth variability, together by the relative water_depthsdepth (h/D), the relative grain size, the Keulegan-Carpenter number and the mobility parameter as the most influential variables governing scour depth variability. Among these, . The analysis across all -the relative water showed the strongest correlation (Fig. 7), OWFs (Fig. 8) showed that where greater relative scour depthsdepth occurred in shallower waters, particularly at location with sediments composed of $(\underline{63} \le d_{50} < \underline{200} \, \mu m \underline{63} \text{ to } \underline{200} \, \mu m)$ and medium sand $(\underline{200} \le d_{50} < \underline{630} \, \mu m \underline{200} \text{ to})$ 630 µm). In shallow waters the increased kinetic energy promotes stronger down-flow and vortex activity around the pile, enhancing scour, whereas in deeper water, hydrostatic pressure dominates, weakening these effects (Melville, 2008; FHWA, 2012), Furthermore, inclusion of the relative grain size captures the effect of grain-pile scaling, while the Keulegan-Carpenter number and the mobility parameter reflect the influence of flow unsteadiness and sediment mobility thresholds, reinforcing their relevance in realistic scour prediction frameworks. This result highlights the critical role of sediment size in scour formation and confirms that finer sediments are more susceptible to hydrodynamic forcing.

(2) Sediment-specific trends correlations: In order to explore the variability within sediment typessoil classes, the data set was clustered according to dP₅₀, and a PCA was applied to each cluster. For fine sand (63 to 200 μm) and medium sand (200 to 630 μm), relative water depthsdepth was found to be the dominant driver of relative scour depthsdepth, demonstrating the sensitivity of these sediment types to hydrodynamic forcing in shallower relative water depthsdepth. For coarser sediments, such as coarse sands (630 to 2000 μm) and fine gravels (2000 to 6300 μm), the correlations were less pronounced, reflecting a greater resistance to scour. This sediment-specific analysis highlights the importance of considering sediment type when assessing scour susceptibility and designing OWFs, and how different sediment types can influence sediment transport patterns.

(3) Site-specific variability: Due to local factors such as sediment conditions, hydrodynamic conditions, and topography, individual OWFs exhibited unique relative scour depthsdepth patterns. For example, London Array (Fig. 1½C) showed trendscorrelations similar to the global results (Fig. 87), with relative water depthsdepth and site topography as the primary influences on scour, followed by current and wave conditions. In contrast, OWFs such as Robin Rigg and Lynn and Inner Dowsing showed no discernible trendscorrelations between relative scour depthsdepth and the key drivers obtained from the global PCA, highlighting the need for individual analyses to account for local complexities.

This study also highlights the potential environmental impacts of scour-induced sediment transport. While the primary focus was on identifying the physical drivers of scour, the findings could provide a first step in assessing potential impacts of OWF on the marine environment due to a changed regional sediment mobility. The entrainment of eroded sediment into the water column, with subsequent long-range transport, raises concerns about sediment deposition and potential impacts on benthic habitats and marine wildlife in far-field regions.

Future research should prioritize the refinement of predictive scour models that incorporate temporal data and expanded hydrodynamic parameters to improve accuracy in diverse sedimentary environments. In addition, integrated approaches that combine regional sediment transport modeling with ecological assessments are critical for evaluating the cumulative impacts of OWF facilities on marine ecosystems. These efforts will facilitate the development of sustainable OWF designs that minimize environmental disturbance while advancing renewable energy goals.

Data availability: The data set used in this study is available in the Marine Data Exchange (MDE) 1038 (https://www.marinedataexchange.co.uk/) and by the Copernicus Marine Service (CMEMS) 1039 (https://marine.copernicus.eu/)

Authors contribution: K. G.: Writing – original draft preparation, visualization, formal analysis, 1042 conceptualization, methodology. **C.J.** Writing – review & editing, supervision, conceptualization, project 1043 administration. **G.M.** Writing – review & editing, resources. **A.S.** Writing – review & editing, methodology. **M.W.** 1044 Writing – review & editing, Supervision. **T.S.** Writing – review & editing, Funding acquisition, Supervision.

- 1045 Competing interests: The authors declare that they have no conflict of interest.
- 1046 Acknowledgements: This work contributes to the DAM Research Mission sustainMare and the project
- 1047 CoastalFutures (Project Number: 03F0911G) funded by the German Federal Ministry of Education and Research
- 1048 (BMBF). The responsibility for the content of this publication lies with the authors.

- 1050 References
- Annad, M., Zourgui, N. H., Lefkir, A., Kibboua, A., and Annad, O.: Scour-dependent seismic fragility curves
- 1052 considering soil-structure interaction and fuzzy damage clustering: A case study of an Algerian RC Bridge
- with shallow foundations, Ocean Engineering, 275, 114157, 2023.
- 1054 Annad, M., Lefkir, A., Mammar-Kouadri, M., and Bettahar, I.: Development of a local scour prediction model
- clustered by soil class, Water Pract. Technol., 16, 1159–1172, 2021.
- 1056 Baykal, C., Sumer, B. M., Fuhrman, D. R., Jacobsen, N. G., and Fredsøe, J.: Numerical investigation of flow and
- scour around a vertical circular cylinder, Philos. Trans. R. Soc. A, 373, 20140104,
- 1058 https://doi.org/10.1098/rsta.2014.0104, 2015.
- 1059 Baelus, L., Bolle, A., and Szengel, V.: Long term scour monitoring around on a sandy seabed, in: Scour and
- 1060 Erosion IX: Proceedings of the 9th International Conference on Scour and Erosion (ICSE 2018), November
- 1061 5–8, 2018, Taipei, Taiwan, CRC Press, 2018.
- 1062 Baeye, M., and Fettweis, M.: In situ observations of suspended particulate matter plumes at an offshore wind farm,
- 1063 southern North Sea, Geo-Mar. Lett., 35, 247–255, 2015.
- 1064 Bailey, H., Brookes, K. L., and Thompson, P. M.: Assessing environmental impacts of offshore wind farms:
- lessons learned and recommendations for the future, Aquat. Biosyst., 10, 1–13, https://doi.org/10.1186/2046-
- 1066 9063-10-8, 2014.
- 1067 Bolle, A., De Winter, J., Goossens, W., Haerens, P., and Dewaele, G.: Scour monitoring around offshore jackets
- and gravity based foundations, in: Proceedings of the Sixth International Conference on Scour and Erosion,
- 1069 Paris, France, 27–31, 2012.
- 1070 Breusers, H. N. C., Nicollet, G., and Shen, H. W.: Local scour around cylindrical piers, J. Hydraul. Res., 15, 211-
- **1071** 252, 1977.
- 1072 Brignon, J. M., Lejart, M., Nexer, M., Michel, S., Quentric, A., Thiebaud, L.: A risk-based method to prioritize
- 1073 cumulative impacts assessment on marine biodiversity and research policy for offshore wind farms in France,
- 1074 Environ. Sci. Pol., 128, 264–276, https://doi.org/10.1016/j.envsci.2021.12.003, 2022.
- 1075 Carpenter, J. R., Merckelbach, L., Callies, U., Clark, S., Gaslikova, L., and Baschek, B.: Potential impacts of
- 1076 offshore wind farms on North Sea stratification, PLOS ONE, 11,
- 1077 https://doi.org/10.1371/journal.pone.0159512, 2016.
- 1078 Carreiras, J., Larroudé, P., Seabra-Santos, F., and Mory, M.: Wave scour around piles, in: Coastal Engineering
- 1079 2000, 1860–1870, 2001.
- 1080 Chen, H., Zhang, J., Guo, Y., Cui, L., Guan, D., and Jiang, L.: Laboratory modelling study on the scour
- 1081 characteristics around a jacket foundation subjected to combined wave-current loading, Renew. Energy,
- **1082** 122443, 2025.
- 1083 Chiew, Y. M.: Local scour at bridge piers, Publication of: Auckland University, New Zealand, 1984.

- 1084 Christiansen, N., Daewel, U., Djath, B., and Schrum, C.: Emergence of large-scale hydrodynamic structures due
- to atmospheric offshore wind farm wakes, Front. Mar. Sci., 64, https://doi.org/10.3389/fmars.2022.818501,
- 1086 2022.
- 1087 CMEMS: Atlantic European North West Shelf Ocean Physics Reanalysis, https://doi.org/10.48670/moi-00059
- 1088 and 10.48670/moi-00060, 2023.
- 1089 Corvaro, S., Mancinelli, A., and Brocchini, M.: Flow dynamics of waves propagating over different permeable
- 1090 beds, Coastal Engineering Proceedings, 35, 35–35, 2016.
- 1091 COWRIE: A Further Review of Sediment Monitoring Data, Cowrie Ltd., Project reference ScourSed-09, 2010.
- 1092 DECC: Dynamics of scour pits and scour protection Synthesis report and recommendations (Milestones 2 and
- 3), Department for Energy and Climate Change, Final Report, 2008.
- 1094 Du, S., Wu, G., Zhu, D. Z., Wang, R., Lu, Y., and Liang, B.: Experimental study of local scour around submerged
- square piles in combined waves and current, Ocean Eng., 266, 113176, 2022.
- 1096 Escarameia, M., and May, R. W. P.: Scour around structures in tidal flows, HR Wallingford, Wallingford, U.K.,
- 1097 1999.
- 1098 EGS (International) Ltd.: Lynn and Inner Dowsing Offshore Wind Farms, Year 3 Post-Construction Survey
- 1099 (2011), Phase 1 Geophysical Survey, Job No. 4918, Final Report Rev 7, CREL Reference No LD-O-EV-
- 1100 013-0000-000000-368-D, Marine Data Exchange, https://www.marinedataexchange.co.uk/details/TCE-
- 1101 1041/2011-egs-lynn-and-inner-dowsing-year-3-post-construction-survey-phase-1---geophysical-
- survey/summary, 2012.
- 1103 EGS (International) Ltd.: Lynn and Inner Dowsing Offshore Wind Farms (October 2012), Job No. 5038, Final
- 1104 Report Rev1, Marine Data Exchange, https://www.marinedataexchange.co.uk/details/TCE-1076/2012-egs-
- lynn-and-inner-dowsing-offshore-wind-farms-post-construction-hydrographic-and-geophysical-
- survey/summary, 2013.
- 1107 EU: An EU Strategy to harness the potential of offshore renewable energy for a climate-neutral future, European
- 1108 Commission, Communication COM/2020/741 final, 2020.
- 1109 Federal Highway Administration (FHWA): Evaluating scour at bridges (HEC-18, Publication No. FHWA-HIF-
- 1110 12-003), U.S. Department of Transportation, 2012.
- 1111
- 1112 Gabriel, K. R.: The Biplot Graphic Display of Matrices with Application to Principal Component Analysis,
- 1113 Biometrika, 58, 453–467, https://doi.org/10.1093/biomet/58.3.453, 1971.
- 1114 Gazi, A. H., Purkayastha, S., and Afzal, M. S.: The equilibrium scour depth around a pier under the action of
- 1115 collinear waves and current, J. Mar. Sci. Eng., 8, 36, 2020.
- 1116 Guşatu, L. F., Menegon, S., Depellegrin, D., Zuidema, C., Faaij, A., and Yamu, C.: Spatial and temporal analysis
- of cumulative environmental effects of offshore wind farms in the North Sea basin, Sci. Rep., 11, 1–18,
- 1118 https://doi.org/10.1038/s41598-021-89537-1, 2021.
- 1119 Harasti, A., Gilja, G., Adžaga, N., and Škreb, K. A.: Principal Component Analysis in development of empirical
- scour formulae, in: Proceedings of the 7th IAHR Europe Congress, Athens, Greece, 7–9 September 2022,
- **1121** 271–272, 2022.
- 1122 Harris, J. M., Herman, W. M., and Cooper, B. S.: Offshore windfarms: an approach to scour assessment, in: Y. M.
- 1123 Chiew, S.-Y. Lim, and N.-S. Cheng (Eds.), Proceedings of the 2nd International Conference on Scour and
- Erosion, Stallion Press, Singapore, 283–291, 2004.

- Harris, J. M., Tavouktsoglou, N. S., Couldrey, A., Whitehouse, R. J., and Klapper, J.: Scour prediction in cohesive
- marine soils: a hybrid approach, ISSMGE Int. J. Geoeng. Case Histories, 7, 59–75, 2023.
- 1127 Harris, J., and Whitehouse, R. J. S.: Scour prediction in non-uniform soils: Undrained shear strength and
- 1128 <u>erodibility</u>, 2014.
- 1129 Hancu, S.: Sur le calcul des affouillements locaux dans la zone des piles de ponts, in: Proceedings of the 14th
- 1130 IAHR Congress, 299–313, 1971.
- 1131 Hjorth, P.: Studies on the nature of local scour, Bull. Ser. A, 46, Department of Water Resources Engineering,
- 1132 <u>Lund Institute of Technology, Sweden, 1975.</u>
- 1133 Hu, R., Wang, X., Liu, H., and Lu, Y.: Experimental study of local scour around tripod foundation in combined
- collinear waves-current conditions, Journal of Marine Science and Engineering, 9(12), 1373, 2021.
- 1135 Jolliffe, I. T., and Cadima, J.: Principal component analysis: a review and recent developments, Philosophical
- 1136 Transactions of the Royal Society A: Mathematical, Physical and Engineering Sciences, 374(2065),
- <u>20150202</u>, <u>2016</u>.
- 1138 Kenyon, N., and Cooper, B.: Sand banks, sand transport and offshore wind farms, Gov. British, 2005.
- 1139 Laursen, E. M.: An analysis of relief bridge scour, J. Hydraul. Div., Proc. ASCE, 89(HY3), 93–118, 1963.
- 1140 Link, O., and Zanke, U.: On the time-dependent scour-hole volume evolution at a circular pier in uniform coarse
 1141 sand, in: Proc. 2nd International Conference on Scour and Erosion (ICSE), 2004.
- 1142 Lloret, J., Turiel, A., Solé, J., Berdalet, E., Sabatés, A., Olivares, A., Gili, J.-M., Vila-Subirós, J., and Sardá, R.:
- 1143 <u>Unravelling the ecological impacts of large-scale offshore wind farms in the Mediterranean Sea, Sci. Total</u>
- Environ., 824, 153803, 2022.
- 1145 1146
- 1147 Louwersheimer, W. F., Verhagen, H. J., and Olthof, J.: Scour around an offshore wind turbine, in: Coastal
- 1148 Structures 2007 Proceedings of the 5th Coastal Structures International Conference, CST07, Venice, Italy,
- 1149 1903–1912, 2009.
- 1150 London Array Ltd.: Environmental Statement Volume 1: Offshore Works, Technical report, London Array Ltd.,
- **1151** 2005.
- 1152 Lyu, X., Cheng, Y., Wang, W., An, H., and Li, Y.: Experimental study on local scour around submerged monopile
- under combined waves and current, Ocean Eng., 240, 109929, 2021.
- 1154 May, R. P., and Willoughby, I. R.: Local scour around large obstructions, HR Wallingford Report SR240, 1990.
- 1155 Matutano, C., Negro, V., López-Gutiérrez, J.-S., and Esteban, M. D.: Scour prediction and scour protections in
- offshore wind farms, Renew. Energy, 57, 358–365, 2013.
- 1157 Matthieu J., Raaijmakers T. Interaction between Offshore Pipelines and Migrating Sand Waves. 2012.
- 1158 McGovern, D. J., Ilic, S., Folkard, A. M., McLelland, S. J., and Murphy, B. J.: Time development of scour around
- a cylinder in simulated tidal currents, J. Hydraul. Eng., 140(6), 04014014, 2014.
- 1160 Melling, G. J.: Hydrodynamic and geotechnical controls of scour around offshore monopiles, University of
- Southampton, Ocean and Earth Science, Doctoral Thesis, 250 pp., 2015.
- 1162 Melville, B.: The physics of local scour at bridge piers, in: Proceedings of the 4th International Conference on
- 1163 Scour and Erosion, 28–38, 2008.
- 1164 Noormets, R., Ernstsen, V., Bartholoma, A., Flemming, B., and Hebbeln, D.: Local scour in a tidal environment:
- a case study from the Otzumer Balje tidal inlet, southern North Sea, Poster reproduced in Appendix A of
- Offshore Center Danmark, 2006, 2003.

- Qi, W. G., and Gao, F. P.: Physical modeling of local scour development around a large-diameter monopile incombined waves and current, Coast. Eng., 83, 72–81, 2014.
- Qi, M., Li, J., and Chen, Q.: Comparison of existing equations for local scour at bridge piers: parameter influence
 and validation, Nat. Hazards, 82, 2089–2105, 2016.
- 1171 Qu, L., An, H., Draper, S., Watson, P., Zhao, M., Harris, J., Whitehouse, R., and Zhang, D.: A review of scour
 1172 impacting monopiles for offshore wind, Ocean Engineering, 301, 117385, 2024.
- 1174 Richardson, M. D., Valent, P., Briggs, K., Bradley, J., and Griffin, S.: NRL mine burial experiments, in:
 1175 Proceedings of the 2nd Australian-American Joint Conference on the Technologies of Mines and Mine
- 1176 Countermeasures, Sydney, Australia, 1–23, 2001.
- 1177 Rivier, A., Bennis, A. C., Pinon, G., Magar, V., and Gross, M.: Parameterization of wind turbine impacts on 1178 hydrodynamics and sediment transport, Ocean Dyn., 66, 1285–1299, 2016.
- 1179 Roulund, A., Sutherland, J., Todd, D., and Sterner, J.: Parametric equations for Shields parameter and wave orbital
- 1180 <u>velocity in combined current and irregular waves, 2016</u>
 1181
- 1182 Rudolph, D., Bos, K. J., Luijendijk, A. P., Rietema, K., and Out, J. M. M.: Scour around offshore structures -
- Analysis of field measurements, in: Y. M. Chiew, S.-Y. Lim, and N.-S. Cheng (Eds.), Proceedings of the 2nd
- 1184 International Conference on Scour and Erosion, Stallion Press, Singapore, 400–407, 2004.
- Saathoff, J. E., Goldau, N., Achmus, M., Schendel, A., Welzel, M., and Schlurmann, T.: Influence of scour and scour protection on the stiffness of monopile foundations in sand, Appl. Ocean Res., 144, 103920, 2024.
- 1187 Sarkar, A.: Scour and flow around submerged structures, in: Proceedings of the Institution of Civil Engineers-
- Water Management, 167(2), 65–78, Thomas Telford Ltd., February 2014.
- 1189 Sarmiento, J., Guanche, R., Losada, I. J., Rosendo, E. M., Guindo, A., and de Guevara, J. L.: Scour processes
- around pile clusters of jacket foundations under steady currents, Ocean Eng., 313, 119502, 2024.
- 1191 Schendel, A.: Wave-current-induced scouring processes and protection by widely graded material, Leibniz
- University Hannover, Dissertation, https://doi.org/10.15488/4453, 2018.
- 1193 Schendel, A., Welzel, M., Schlurmann, T., and Hsu, T.-W.: Scour around a monopile induced by directionally
- spread irregular waves in combination with oblique currents, Coast. Eng., 161, 103751,
- https://doi.org/10.1016/j.coastaleng.2020.103751, 2020.
- 1196 Schultze, L. K. P., Merckelbach, L. M., Horstmann, J., Raasch, S., and Carpenter, J. R.: Increased mixing and
- turbulence in the wake of offshore wind farm foundations, J. Geophys. Res. Oceans, 125(8), e2019JC015858,
- **1198** 2020.

1210

- 1199 Sheppard, D. M., Odeh, M., and Glasser, T.: Large scale clear-water local pier scour experiments, J. Hydraul.
- 1200 Eng., 130(10), 957–963, 2004.
- 1201 Shields, M. A., Woolf, D. K., Grist, E. P., Kerr, S. A., Jackson, A. C., Harris, R. E., and Side, J.: Marine renewable
- energy: The ecological implications of altering the hydrodynamics of the marine environment, Ocean Coast.
- 1203 Manag., 54(1), 2–9, 2011.
- Sheppard, D. M., Zhao, G., and Ontowirjo, B.: Local scour near single piles in steady currents, in: Water Resources
 Engineering, pp. 1809–1813, ASCE, 1995.
- Sheppard, D. M., Ontowirjo, B., and Zhao, G.: Conditions of Maximum Local Scour, in: Proceedings of Stream
 Stability and Scour at Highway Bridges, Resources Engineering Conference 1991–1998, edited by
- Richardson, E. V., and Lagasse, P. F., ASCE, Reston, VA, 1999.

- 1211 Smith, J. D., and McLean, S. R.: Spatially averaged flow over a wavy surface, J. Geophys. Res., 82(12), 1735-
- **1212** 1746, 1977.
- 1213 Soulsby, R. L., and Whitehouse, R. J. S.: Threshold of sediment motion in coastal environments, in: Pacific Coasts
- and Ports '97: Proceedings of the 13th Australasian Coastal and Ocean Engineering Conference and the 6th
- Australasian Port and Harbour Conference, Vol. 1, pp. 145–150, Centre for Advanced Engineering, University
- of Canterbury, Christchurch, NZ, 1997.
- 1217
- 1218 Soulsby, R.: Dynamics of Marine Sands, Thomas Telford Ltd., 1997.
- 1219 Stahlmann, A.: Numerical and experimental modeling of scour at foundation structures for offshore wind turbines,
- in: ISOPE International Ocean and Polar, June 2013.
- 1221 Sturt, F., Dix, J. K., and EMU Ltd.: The Outer Thames Estuary Regional Environmental Characterisation, Marine
- Aggregate Levy Sustainability Fund, 09/J/1/06/1305/0870, Technical report, Marine Aggregate Levy
- 1223 Sustainability Fund, 2009.
- 1224 Sumer, B. M., Fredsøe, J., and Christiansen, N.: Scour around vertical pile in waves, J. Waterway Port Coastal
- 1225 Ocean Eng., 118, 15, 1992.
- 1226 Sumer, B. M., and Fredsøe, J.: Scour around pile in combined waves and current, J. Hydraul. Eng., 127(5), 403-
- **1227** 411, 2001.

- 1228 Sumer, B. M., Petersen, T. U., Locatelli, L., Fredsøe, J., Musumeci, R. E., and Foti, E.: Backfilling of a scour hole
- around a pile in waves and current, J. Waterway, Port, Coastal, Ocean Eng., 139(1), 9–23, 2013.
- 1231 Teilmann, J., and Carstensen, J.: Negative long term effects on harbour porpoises from a large scale offshore wind
- farm in the Baltic evidence of slow recovery, Environ. Res. Lett., 7, https://doi.org/10.1088/1748-
- **1233** 9326/7/4/045101, 2012.
- 1234 Van Rijn, L. C.: Sediment transport, part I: bed load transport, J. Hydraul. Eng., 110(10), 1431–1456, 1984.
- 1235 Vanhellemont, Q., and Ruddick, K.: Turbid wakes associated with offshore wind turbines observed with Landsat
- 1236 8, Remote Sens. Environ., 145, 105–115, 2014.
- 1237 Walker, W.: Field measurements of local pier scour in a tidal inlet, MSc, University of Florida, 1995.
- 1238 Watson, S. C., Somerfield, P. J., Lemasson, A. J., Knights, A. M., Edwards-Jones, A., Nunes, J., and Beaumont,
- 1239 N. J.: The global impact of offshore wind farms on ecosystem services, Ocean Coast. Manag., 249, 107023,
- 1240 https://doi.org/10.1016/j.ocecoaman.2024.107023, 2024.
- 1241 Welzel, M., Schendel, A., Schlurmann, T., and Hildebrandt, A.: Volume-based assessment of erosion patterns
- around a hydrodynamic transparent offshore structure, Energies, 12(16), 3089, 2019.
- 1243 Welzel, M.: Wave-current-induced scouring processes around complex offshore structures, 2021.
- 1244 Welzel, M., Schendel, A., Satari, R., Neuweiler, I., and Schlurmann, T.: Spatio-temporal analysis of scour around
- complex offshore foundations under clear water and live bed conditions, Ocean Eng., 298, 117042, 2024.
- 1246 Wilson, J. C., and Elliott, M.: The habitat-creation potential of offshore wind farms, Wind Energy, 12(2), 203-
- **1247** 212, 2009.
- 1248 Whitehouse, R.: Dynamics of estuarine muds. Thomas Telford, 2000.
- 1249 Whitehouse, R. J. S., Harris, J. M., Mundon, T. R., and Sutherland, J.: Scour at offshore structures, in: Proceedings
- of the 5th International Conference on Scour and Erosion, San Francisco, 11–20, 2010.
- 1251 Whitehouse, R. J. S., Harris, J. M., Sutherland, J., and Rees, J.: The nature of scour development and scour
- protection at onshore wind farm foundations, Mar. Pollut. Bull., 62(1), 73–88, 2011.

1253	Whitehouse, R. J. S., and Harris, J.: Scour prediction offshore and soil erosion testing, HR Wallingford Report,
1254	<u>2014.</u>
1255	Yao, Y., Chen, Y., Zhou, H., and Yang, H.: Numerical modeling of current loads on a net cage considering fluid-
1256	structure interaction, J. Fluids Struct., 62, 350–366, 2016.
1257	Zhao, M., Zhu, X., Cheng, L., and Teng, B.: Experimental study of local scour around subsea caissons in steady
1258	currents, Coast. Eng., 60, 30-40, 2012.
1259	Zanke, U. C. E., Hsu, TW., Roland, A., Link, O., and Diab, R.: Equilibrium scour depths around piles in
1260	noncohesive sediments under currents and waves, Coastal Eng., 58(10), 986-991, 2011.
1261	